https://doi.org/10.5194/bg-2020-1
Preprint. Discussion started: 31 January 2020

Biogeosciences Discussions

Interactive impacts of meteorological and hydrological conditions on the physical and biogeochemical structure of a coastal system

Onur Kerimoglu[1,2], Yoana G. Voynova[1], Fatemeh Chegini[3], Holger Brix[1], Ulrich Callies[1], Richard Hofmeister[1], Knut Klingbeil[3], Corinna Schrum[1], and Justus E.E. van Beusekom[1]

[1]Institute for Coastal Research, Helmholtz-Zentrum Geesthacht, Germany
[2]Institute for Chemistry and Biology of the Marine Environment, Carl von Ossietzky University Oldenburg, Germany
[3]Leibniz Institute for Baltic Sea Research, Warnemünde, Germany

Correspondence: Onur Kerimoglu (kerimoglu.o@gmail.com)

Abstract. The German Bight was exposed to record high riverine discharges in June 2013, as a result of flooding of the Elbe and Weser rivers. Several anomalous observations suggested that the hydrodynamical and the biogeochemical state of the system was impacted by this event. In this study, we developed a biogeochemical model and coupled it with a previously introduced high resolution hydrodynamical model of the southern North Sea, in order to better characterize these impacts, and gain insight into the underlying processes. Performance of the model was assessed using an extensive set of *in-situ* measurements for the period 2011-2014. We first improved the realism of the hydrodynamic model with regard to the representation of cross-shore gradients, mainly through inclusion of flow-dependent horizontal mixing. Among other characteristic features of the system, the coupled model system can reproduce the low salinities, high nutrient concentrations and low oxygen concentrations in the bottom layers observed within the German Bight following the flood event. Through a scenario analysis, we examined the sensitivity of the patterns observed during July 2013 to the hydrological and meteorological forcing in isolation. Within the region of freshwater influence (ROFI) of the Elbe-Weser rivers, the flood event clearly dominated the changes in salinity and nutrient concentrations, as expected. However, our findings point out to the relevance of the peculiarities in the meteorological conditions in 2013 as well: a combination of low wind speeds, warm air temperatures and cold bottom water temperatures resulted in a strong thermal stratification in the outer regions, and limited vertical nutrient transport to the surface layers. Within the central region, the thermal and haline dynamics interactively resulted in an intense density stratification. This intense stratification, in turn, led to enhanced primary production within the central region enriched by nutrients due to the flood, but reduction within the nutrient-limited outer region, and it caused a wide-spread oxygen depletion in bottom waters. Our results further point to the enhancement of the current velocities at the surface as a result of haline stratification, and intensification of the thermohaline estuarine-like circulation at the Wadden Sea, both driven by the flood event.

https://doi.org/10.5194/bg-2020-1
Preprint. Discussion started: 31 January 2020

1 Introduction

Riverine discharges influence the thermohaline stratification, nutrient availability and as a result, primary production within the coastal zones (e.g., Hickey et al., 2010; Cloern et al., 2014; Emeis et al., 2015). Excess amounts of riverine nutrient inputs cause coastal eutrophication, associated with a host of problems (Smith and Schindler, 2009), including development of dense and harmful algal blooms (e.g., Garnier et al., 2019), decline of submerged vegetation (e.g., Dolch et al., 2013), and oxygen depletion (see the review by Fennel and Testa, 2019). Fraction of riverine freshwater and nutrients that reaches the open ocean is an open question, with estimates ranging between 15% and 80 % (Sharples et al., 2017; Izett and Fennel, 2018).

Mixing of riverine freshwater with the surrounding saline marine waters at the coasts is driven by a set of hydrodynamical processes intriguingly linked together (for a recent review, see Geyer and Maccready, 2014). The freshwater inputs by rivers may lead to haline stratification in the coastal region, in the absence of any thermal stratification (van Aken, 1986). Horizontal density gradients caused by riverine freshwater inputs govern gravitational circulation (i.e., exchange flow) where the seaward flow of the lighter water at the surface is counteracted by a landward flow of the saltier, denser waters near the sea floor (see Burchard et al., 2018). Destabilizing and stabilizing effects of flood and ebb currents, respectively, may further enhance the gravitational circulation (Burchard and Hetland, 2010).

The study system, the German Bight, is a shallow area located in the southeastern North Sea (Fig.1). The prevailing wind direction is southwesterly (Siegismund and Schrum, 2001), governing a large cyclonic gyre within the southern North Sea (Sündermann and Pohlmann, 2011). But under easterly and northeasterly winds, anticyclonic circulation may prevail (Becker et al., 1992; Dippner, 1993; Callies et al., 2017). Occurrence of thermohaline stratification within the German Bight is driven by the the buoyancy inputs from the rivers to the coastal waters and the heat fluxes at the deeper areas (Frey, 1990; Simpson et al., 1993). It is also strongly influenced both by the intensity and direction of wind: while the westerly winds allow, and the easterly winds enhance stratification, southerly winds have a particularly destratifying effect (Schrum, 1997). An estuarine-like circulation has been shown to be present within the coastal areas of the German Bight (Burchard et al., 2008; Burchard and Badewien, 2015). This mechanism has been suggested to contribute to the maintenance of the steep, cross-shore suspended particulate matter (SPM) and nutrient gradients (Flöser et al., 2011; Hofmeister et al., 2017), with regional differences (van Beusekom et al., 2019). The steep cross-shore gradients observed in SPM and nutrient concentrations have been recently reproduced by numerical models (Staneva et al., 2009; Gräwe et al., 2016) owed to high resolution grids and the terrain-following vertical coordinates that enables representation of the estuarine circulation.

Surrounded by industrialized and densely populated countries, the southern North Sea has been experiencing eutrophication related problems (Radach, 1992; Hickel et al., 1993; OSPAR, 2017) such as occasional oxygen depletion events during summer (Frey, 1990; Große et al., 2016). Elbe and Weser rivers have been estimated to be primary sources of nitrogen (N) in the southern North Sea (Große et al., 2017). Since the 1980s, nutrient concentrations in these and other contributing rivers (e.g., Rhine, Meuse), have been significantly reduced, more for phosphorus (P) than for N (Radach and Pätsch, 2007), which resulted in some improvement especially within the northern Wadden Sea (Wiltshire et al., 2008; van Beusekom et al., 2019), but

https://doi.org/10.5194/bg-2020-1
Preprint. Discussion started: 31 January 2020

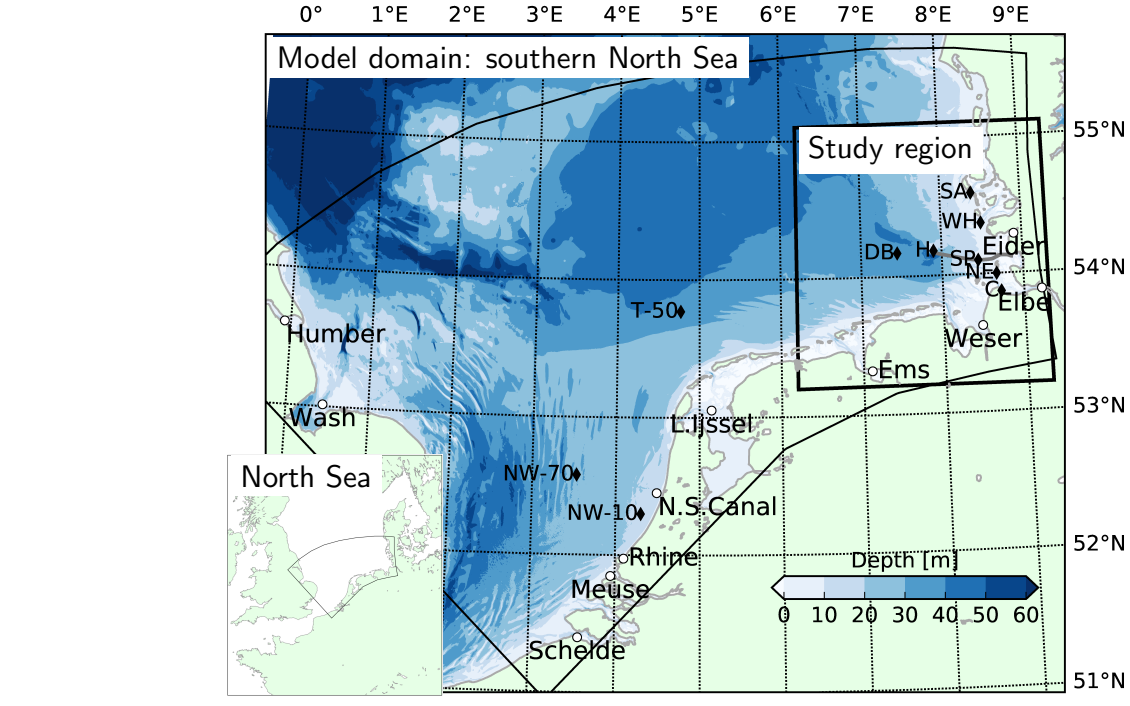

Figure 1. Model domain, bathymetry (data from the European Marine Observation and Data Network, EMODnet), and the location of the study region, the German Bight. Filled circles: location of river mouths on the grid, diamonds: monitoring stations (NW: Noordwijk, T: Terschelling, DB: Deutsche Bucht, H: Helgoland, SP: Suederpiep, SA: Southern Amrum, WH: Westerhever, NE: Norderelbe, C:Cuxhaven), gray line: the average route of the Ferrybox transect between Helgoland and Büsum (see section 2.3).

according to a recent study, the nutrient concentrations within the coastal areas are estimated to be still 50-70% higher in comparison to the pre-industrial state of the 1880s (Kerimoglu et al., 2018).

The extent to which the hydrodynamical structure, and the transport of riverine material within the German Bight depends on the inter-annual variability in riverine discharges is not fully understood. In particular, whether and to what extent a flood event would influence the thermohaline stratification within the off-shore waters, or the estuarine circulation at the coastal waters has not been explicitly investigated. In this study, based on the simulations obtained with a coupled physical-biogeochemical model, we examine the physical and biogeochemical structure in the German Bight during July 2013, i.e., following a major flood event (Voynova et al., 2017), in comparison to those in the previous year, July 2012, in order to characterize the sensitivity of the hydrodynamical and biogeochemical structure within the German Bight to the meteorological and hydrological conditions. Through a numerical scenario analysis, we try to disentangle the effects of the flood event, meteorology, and in particular the wind conditions.

https://doi.org/10.5194/bg-2020-1
Preprint. Discussion started: 31 January 2020


Biogeosciences Discussions

2 Material & Methods

2.1 The Model

The hydrodynamical host, the General Estuarine Transport Model (GETM, Burchard and Bolding, 2002) is a free-surface baroclinic model that uses terrain-following vertical coordinates. GETM was previously applied to the greater North Sea area (Stips et al., 2004; Pätsch et al., 2017) and the German Bight and Wadden Sea regions in higher resolution (Staneva et al., 2009; Gräwe et al., 2016). In the current application, GETM is defined on a curvilinear grid with a resolution of 1.5-4 km (Fig. 1) and 20 vertical layers, and operated with integration time steps of 5 s and 360 s for the barotropic and baroclinic modes, respectively. At the northern and western boundaries, surface elevations extracted from TRIM-NP-2D (Gaslikova and Weisse, 2013) are provided as clamp boundary conditions at hourly resolution (see below for other boundary conditions). For the discretization of advection, we employed a third order, total variation diminishing P2-PDM (i.e., ULTIMATE QUICKEST) scheme, recognized for its accuracy and gradient conserving qualities (e.g., Pietrzak, 1998; Burchard and Rennau, 2008).

An almost identical model setup was previously employed and shown to capture the spatial and temporal distributions of temperature and salinity within the German Bight for the period 2000-2010 (Kerimoglu et al., 2017a), as well as the tidal dynamics (Nasermoaddeli et al., 2017). Since then, the following refinements were made: *i*) providing meteorological forcing at hourly resolution extracted from a COSMO-CLM hindcast simulation (Geyer, 2014), which was previously at 6-hr resolution; and *ii*) specifying the monthly average vertical temperature and salinity profiles at the boundaries for each year separately as predicted by HAMSOM (for a recent description of the setup, see Große et al., 2017), instead of providing climatological averages for all years; *iii*) explicitly describing the horizontal diffusion through Smagorinsky parameterization (Smagorinsky, 1963). Impacts of the first two refinements *i-ii* were subtle and local, but introduction of the horizontal diffusion systematically improved the representation of coastal gradients, and resulted in more plausible total mixing rates overall (see Appendix A).

The biogeochemical model employed here has been recently developed. It has two main components: a component that describes plankton dynamics, and a geochemistry component that describes the recycling of the organic material within the water and sediments. These compartments, both of which are implemented as FABM (Framework for Aquatic Biogeochemical Models, Bruggeman and Bolding (2014)) modules, are coupled in run-time. Elemental fluxes between various model compartments are illustrated in Fig. 2.

The plankton component has been developed based on the carbon (C-) and P- resolving generic plankton model described by Kerimoglu et al. (2017b) in the context of a lake application. Specifically, the extensions included descriptions of N and silicate (Si) limitation of phytoplankton (diatoms for the latter), and variations of the Chl:C ratio according to Geider et al. (1997). Heterotrophs can now handle and properly recycle prey with constant or variable C:N:P:Si ratios. The 'genericity' of the previous model version (Kerimoglu et al., 2017b) was due to the fact that each plankton species was described as a potential mixotroph with a prescribed autotrophy/heterotrophy ratio. In the new version, explicit phytoplankton and zooplankton modules are used, in order to facilitate future development, where phytoplankton-, zooplankton- and mixotroph- specific functionalities are foreseen to be included in future work. In the present application, plankton comprises two phytoplankton functional groups, namely diatoms and nanoflagellates, and two zooplankton functional groups, namely, micro- and meso-zooplankton.

https://doi.org/10.5194/bg-2020-1
Preprint. Discussion started: 31 January 2020

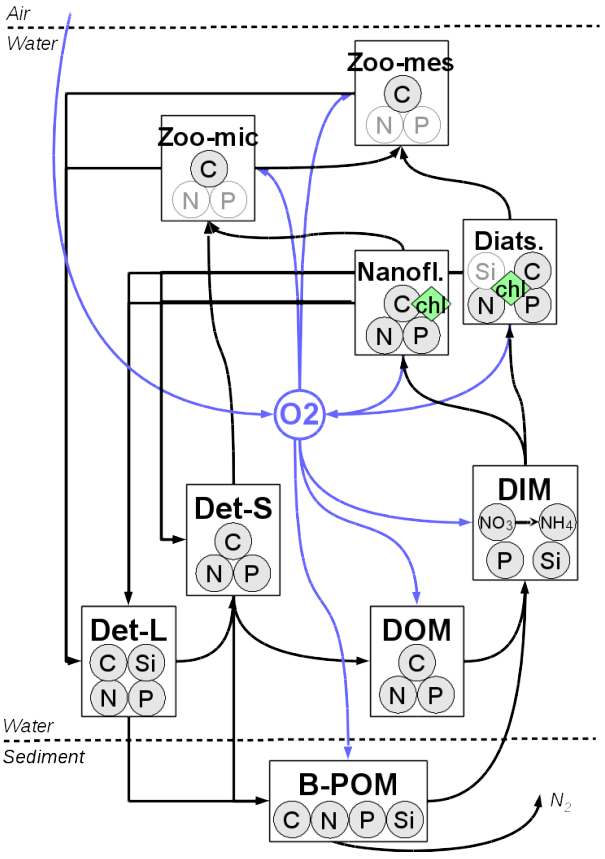

Figure 2. Elemental fluxes between model compartments. Det-L and Det-S: Large and Small detritus, DOM: Dissolved Organic Matter, DIM: Dissolved Inorganic Matter, B-POM: Benthic Particulate Organic Matter. The pale N and P in micro- and mesozooplankton and Si in diatoms represent diagnostic state variables which are determined by a fixed prescribed ratio to the C-bound to these pools, resolved as a state variable.

The abiotic (geo-chemistry) component is based on ECOHAM, as described by Lorkowski et al. (2012). This component describes the dynamics of two detritus size classes, a dissolved organic material (DOM) pool, a dissolved inorganic material (DIM) pool, a 0-D benthic pool and dissolved oxygen. Light conditions are determined by the shading by detritus, DOM and a parameterization of background turbidity caused by SPM. A detailed description of the model formulations and parameters can be found in Appendix B.

Starting from the initial conditions obtained earlier, the model was spun-up for the period 2008-2010 with the parameterization presented here, as up to 3 years was found to be necessary for the solutions to converge from arbitrary initial conditions. We then consider the period 2011-2014 for the model performance assessment. For the analysis of the years 2012 and 2013, in addition to the reference run, we consider three scenarios in order to investigate the sensitivity of the physical and biogeochemical structure of the system to the meteorological and hydrological forcing: based on the 2013 run (with respect to ocean

https://doi.org/10.5194/bg-2020-1
Preprint. Discussion started: 31 January 2020

boundary and initial conditions), the scenario '2013-R12' was ran with the river forcing of 2012, '2013-M12' was run with the meteorological forcing of 2012. In a third scenario, '2013-W12', only the June-August 2013 was simulated with the wind and atmospheric pressure fields from 2012, starting from the initial conditions of June 2013 and using the ocean boundary conditions of 2013.

2.2 Riverine and Atmospheric Data

Both for atmospheric forcing of the coupled physical-biogeochemical model, and for the analysis of meteorological conditions, we use an atmospheric hindcast with a 0.22° resolution (Geyer, 2014). Atmospheric deposition of nitrogen was downloaded from the website of the European Monitoring and Evaluation Programme. Riverine fluxes were maintained and provided by S. van Leeuwen (NIOZ) upon personal request. Variability of discharge rates and concentration of inorganic and organic constituents for the period have been explored by Radach and Pätsch (2007). Small (<30d) gaps in riverine data were filled using linear interpolation, and larger gaps were replaced with long-term (2000-2017) climatologies.

2.3 Observation data

Station data (Helgoland, Cuxhaven, Deutsche Bucht (German Bight), see Fig.1 for the locations) for temperature, salinity and oxygen (latter only at Deutsche Bucht) were downloaded from the COSYNA (Coastal Observing System for Northern and Arctic Seas) data portal (www.cosyna.de, see Breitbach et al., 2016) at daily resolution (snapshots at 00:00 averaged within a 3600 s time window). Collection and processing of the semi-continuous data collected by FerryBox platforms at the Cuxhaven and Helgoland monitoring stations and on the M/V *Funny Girl* ferry operating between Büsum and Helgoland during May-September have been described previously by Petersen et al. (2011) and Voynova et al. (2017) and are available from the COSYNA data portal as well.

N, P, Si and chlorophyll data at the Helgoland-Roads station was collected at semi-daily (every working day), and using standard procedures as described by Wiltshire et al. (2008). Data from the Noordwijk, Terschelling, Norderelbe, Suederpiep and Westerhever stations are available at monthly intervals. For the Noordwijk-70 and Terschelling-50 stations, we consider only the surface measurements available at biweekly intervals, while the data at other stations are located at shallow sites, therefore provide only surface measurements. Mooring data for surface (<10 m) salinity, temperature and nutrients, randomly distributed over the entire model domain and simulation period 2011-2014, were obtained from the International Council for the Exploration of the Sea (ICES). In this dataset, the outliers, defined as the values falling outside the $[\bar{o} \pm 4\sigma]$ range, where $\bar{o}$ and σ stand for the mean and standard deviation of the raw observations were removed.

Spatial matching of all data was performed by calculating the distance-weighted mean of the nearest four modelled grid values around the observation, using the 'spatial.cKDTree' package from the Scipy library of Python 3.5.

https://doi.org/10.5194/bg-2020-1
Preprint. Discussion started: 31 January 2020

Biogeosciences Discussions Open Access EGU

3 Results

3.1 Hydrological and Meteorological Conditions

Typically, the discharge rates of the continental rivers around the southern North Sea peaks during winter/early spring (e.g., Lenhart et al., 1997). Flow rates of Elbe, Weser and Ems during 2012 and 2013 follow this typical pattern (Fig.3) but during June 2013, a large precipitation event over the central Europe caused flooding of all major river basins in Germany (Merz et al., 2014), including Elbe and Weser (Fig.3). The Elbe flood ocan be considered as a 100-year event with discharge rates of up to 4060 m^3 s^{-1} during 11 and 12 June (Voynova et al., 2017). Nitrogen, phosphorus and silicate fluxes paralleled the discharge rates, with distinct peaks during June 2013 for the Elbe and Weser rivers (Fig.3).

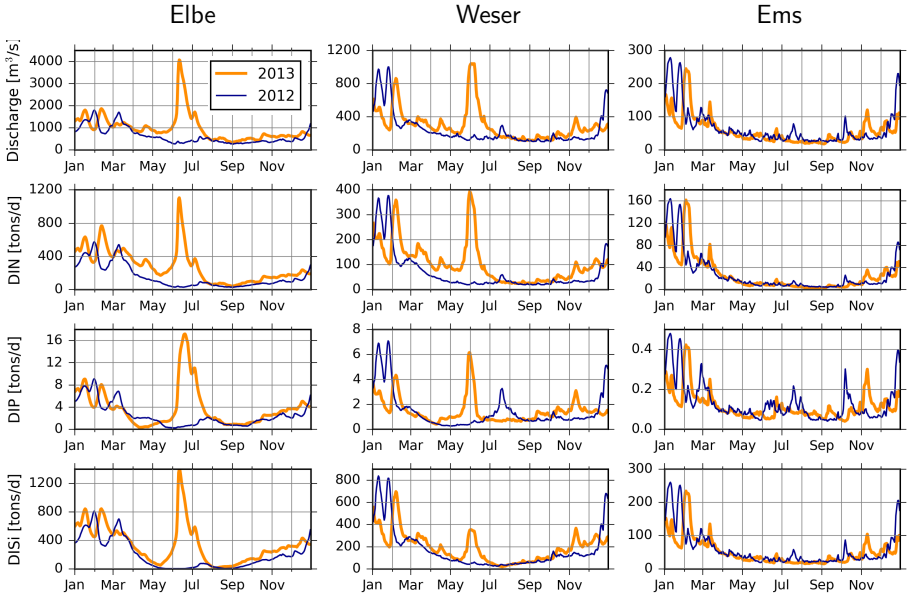

Figure 3. Measured discharge, DIN (NO3+NH4), DIP and DISi loading rates at rivers Elbe, Weser, and Ems during 2012 (dashed blue lines) and 2013 (red lines).

Meteorological conditions during 2012 and 2013 differed systematically during two periods (Fig. 4). The first of these occurred during the early spring: March 2012 was characterized by relatively warm air temperatures and winds mildly blowing from the west/southwest, whereas March 2013 was cold with strong easterly winds. The second period occurred during the middle of summer: July 2012 was relatively cold with overcast skies and some precipitation, contrasting with warmer, drier and calmer conditions in July 2013.

https://doi.org/10.5194/bg-2020-1
Preprint. Discussion started: 31 January 2020

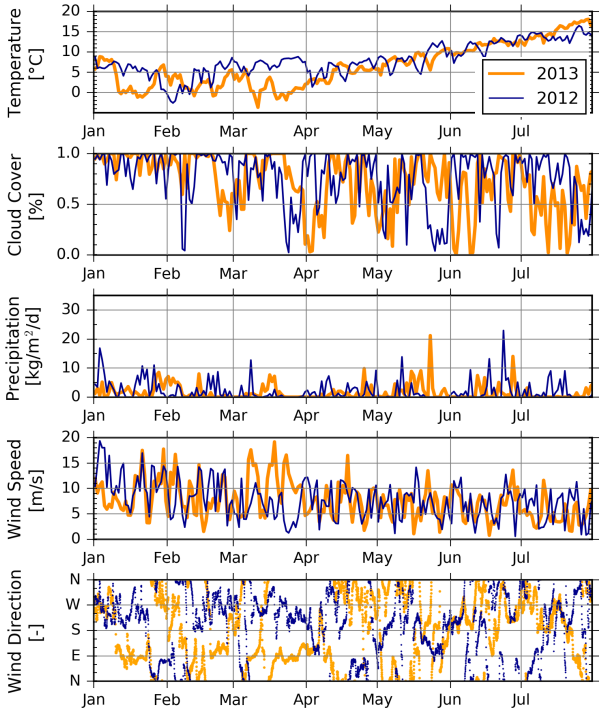

Figure 4. Meteorological variables during January-July 2012 and 2013, extracted from a representative grid point (54°14'N, 7°29'E) of the meteorological hindcast, used also as model forcing (see Section 2.2). Temperature is from 2 m and wind is from 10 m height above the sea level. Wind direction is shown at hourly resolution, all other variables at daily resolution.

3.2 Assessment of the Model Performance

Simulated temperature and salinities at the surface match well to the observations found in the ICES database, randomly distributed throughout the model domain within the period 2011-2014 (Fig. 5), and exhibit no signs of systematic deviations or biases. Match of the simulated NO3 and DIP to the ICES-observation set is reasonably well, with -5% normalized bias and correlation coefficients larger than 0.6 for both variables (Fig. 5).

Comparison of simulated and measured temperature and salinity at 3 fixed monitoring stations are shown in Fig. 6. Two of these stations, Helgoland and Cuxhaven are located at shallow sites, therefore provide only surface measurements, whereas the third one, the Deutsche Bucht, provides measurements also at 30m depth. At all these stations, temperature is estimated with 5-9% negative bias, and correlation scores ranging between 0.99-1.0. The inter-annual variations are well captured: the relatively warm winters (January-March) of 2012 and 2014, and the cold winter of 2013 manifest as cold and warm water temperatures according to the observations, and these differences are realistically reproduced by the model, despite the modeled temperatures being about 0.5 to 1.0 K lower. Salinity is modelled consistently with only up to 2% bias at all 3 stations, despite the relatively lower correlation coefficients in comparison to temperature (Fig.6). The relatively higher variability of the salinity

https://doi.org/10.5194/bg-2020-1
Preprint. Discussion started: 31 January 2020

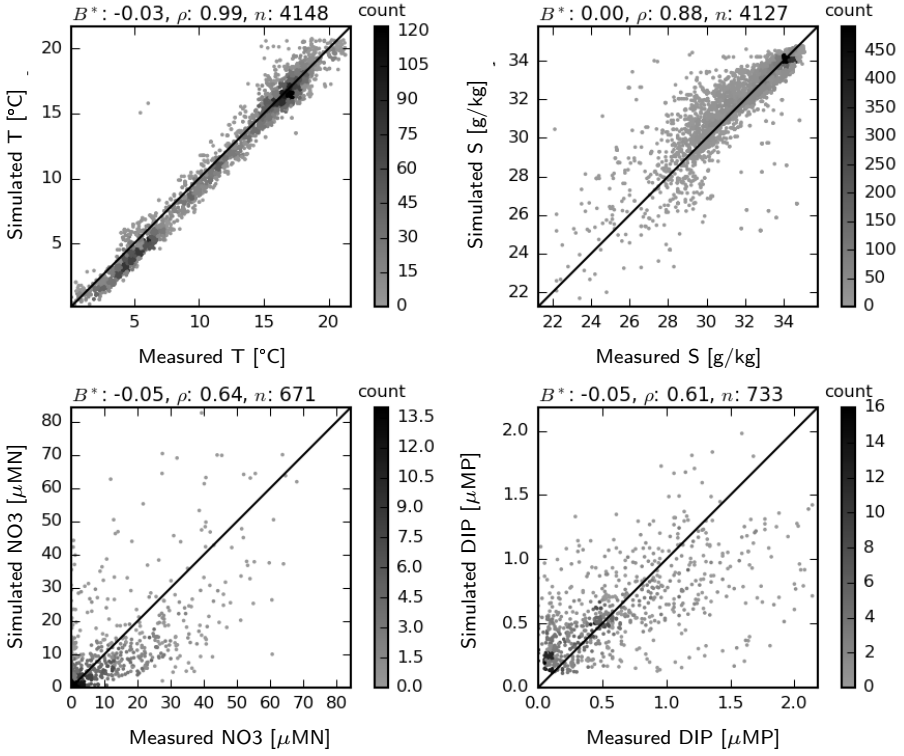

Figure 5. Simulated vs measured temperature, salinity, NO3 and DIP at the surface for the period 2011-2014

measurements are due to the tidal variations (most obvious at the Cuxhaven station), which are smeared out in the daily average model output. The freshwater plume of the flood event of June 2013, and other similar events have been accurately reproduced by the model.

According to the June-July average salinities measured by FerryBox on the M/V *Funny Girl* ferry on its transect between Büsum and Helgoland (Fig.1), the salinities gradually decrease from about 32 g/kg at Helgoland to about 27 g/kg at Büsum in 2012 (Fig. 7). In 2013, driven by the freshwater plume of the flood, the average salinities were lower at both edges, with about 27-29 g/kg at Helgoland and 22-23 g/kg at Büsum. The model estimates are quite accurate at the off-shore areas, but undershoot the observations near the coast, up to 2 g/kg in 2012 and 3-5 g/kg in 2013. Despite these biases, the clear difference between the two years as captured by the FerryBox is qualitatively captured by the model.

Dissolved inorganic N (DIN, which in our model comprise NO3 and NH4, as NO2 was not considered) and P (DIP, i.e., PO4) are generally well reproduced at all monitoring stations considered (Fig.8), as suggested by low bias and moderate correlations. The ability of the model to capture the sharp increase in DIN during June/July 2013 at the Helgoland station suggests that the spreading of the plume of the Elbe-Weser rivers following the flood event was realistically reproduced. For dissolved silicate, DISi, model estimates overshoot the observations by about 50% at Helgoland and up to 100% at the Noordwijk stations. Latter is mainly driven by the strong DISI fluxes from the western boundary (Fig. 1).

https://doi.org/10.5194/bg-2020-1
Preprint. Discussion started: 31 January 2020

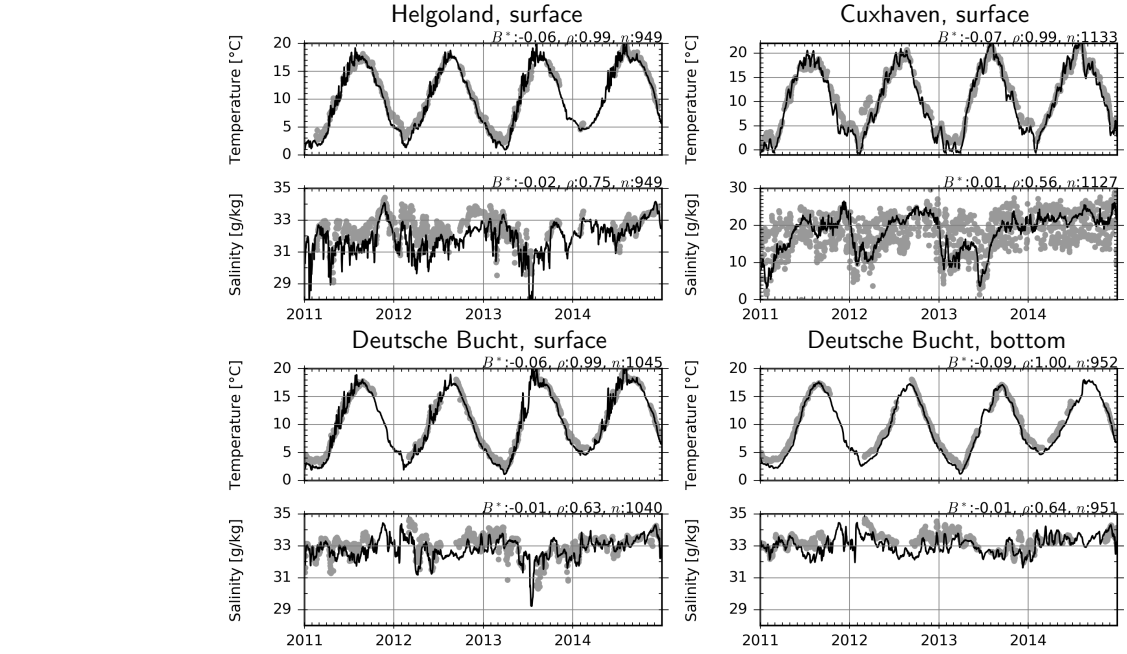

Figure 6. Observations (dots) and model estimates (lines) of temperature and salinity. $B*$: normalized bias, ρ: correlation coefficient, n: number of observation-simulation pairs.

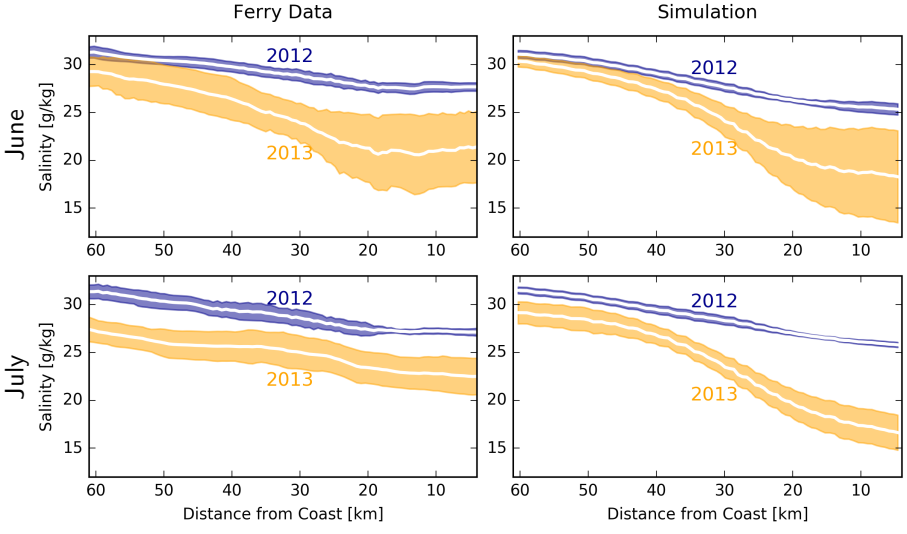

Figure 7. Average and standard deviation of salinities between Helgoland and Büsum, according to the FerryBox data from M/V *Funny Girl* and simulation by the model during June and July 2012 and 2013.

https://doi.org/10.5194/bg-2020-1
Preprint. Discussion started: 31 January 2020

Biogeosciences
Discussions
Open Access
EGU

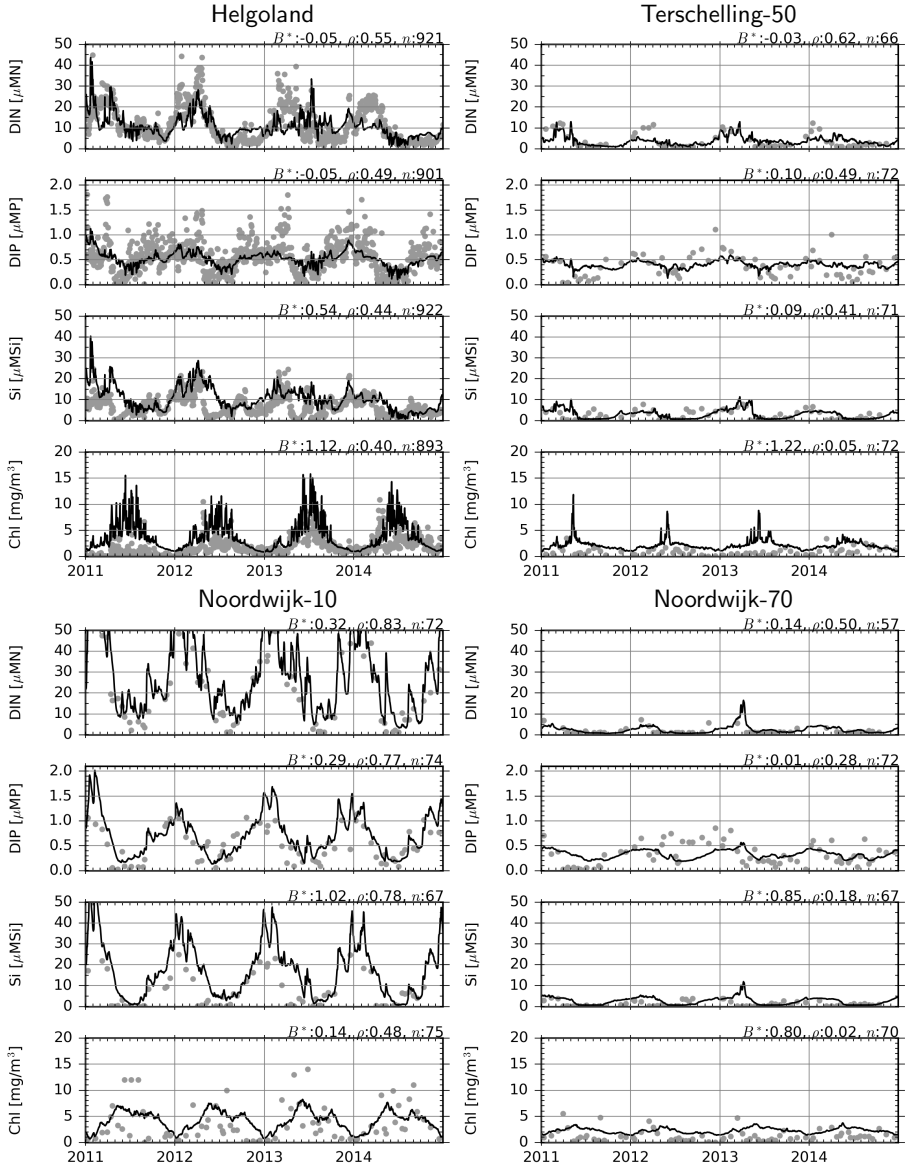

Figure 8. Observations (dots) and model estimates (lines) of surface DIN, DIP, DISi and chlorophyll concentrations. $B*$: normalized bias, ρ: correlation coefficient, n: number of observation-simulation pairs.

For chlorophyll, there is up to 120% positive bias at the off-shore stations (Fig.8), while the correlation coefficients are particularly low at the Terschelling-50 and Noordwijk-70 stations and moderate at Helgoland and Noordwijk-10. A consistent source of error seems to be the failure of the model to estimate the timing of the spring bloom. However, differences between

https://doi.org/10.5194/bg-2020-1
Preprint. Discussion started: 31 January 2020

stations, i.e., values at Helgoland and Noordwijk-10 being higher than at Terschelling-50 and Noordwijk-70 stations, are well reproduced.

Measured and simulated NO3 and DIP concentrations at 3 coastal stations, Norderelbe, Suederpiep and Westerhever, located along the North-Frisian Wadden Sea (Fig. 1), are shown in Fig. 9. For the NO3, measurements in both June and July 2013 were distinctly higher than those in 2012 at Norderelbe and Suederpiep stations, but not at Westerhever in July. Despite a tendency to overshoot, range of simulated values mostly enclose the measurements, and the qualitative differences between 2012 and 2013 and among different stations were captured by the model. Average DIP measurements did not differ between 2012 and 2013, but gradually decreased with distance to the Elbe mouth. The model captures this gradual decline with distance, but the difference it suggests between the two years at the Norderelbe and Suederpiep station in July is larger than the measurements.

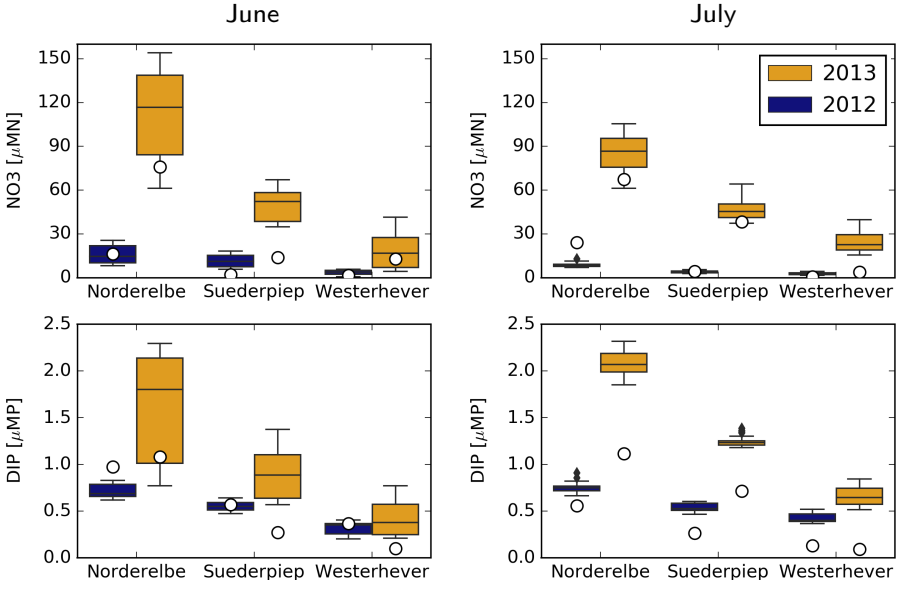

Figure 9. Monthly average measurements (circles) and temporal distribution of the simulations (boxes showing the median, 1st and 3rd quartile and whiskers showing the minimum and maximum values) for surface NO3 and DIP concentrations at three coastal stations shown in Fig. 1.

3.3 Thermohaline structure, nutrient status and productivity of the system

Average salinities in the surface and bottom layers estimated by the model suggest considerable extension of the Elbe-Weser ROFI during July 2013, in comparison to July 2012 (Fig. 10). This extension is similar in surface and bottom layers within the well mixed shallow areas, but stronger at the surface in deeper regions where a thermohaline stratification develops (Fig. 11). The surface and bottom temperatures display similar horizontal gradients during July 2012 and 2013 with higher temperatures near the coast, and lower temperatures within the offshore regions (Fig. 10). However, the surface temperatures within the outer

https://doi.org/10.5194/bg-2020-1
Preprint. Discussion started: 31 January 2020

areas during July 2013 are 1-2 K higher than those during July 2012 (Fig. 4). In contrast, the bottom temperatures during 2013 July are lower than those during July 2012.

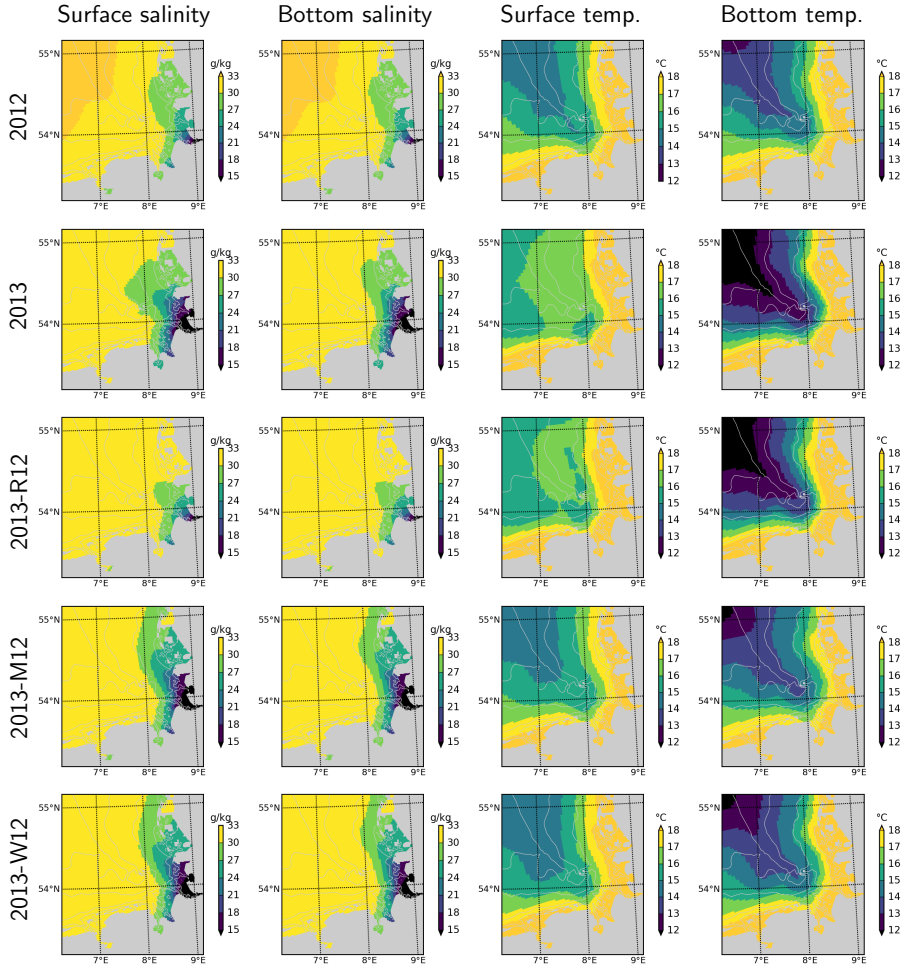

Figure 10. Salinity and temperature in the surface and bottom layers during July for the years 2012 and 2013 and scenarios 2013-R12, 2013-M12 and 2013-W12.

When the riverine forcing of 2012 was used for simulating 2013 ('2013-R12' scenario), the characteristic freshwater plume of 2013 disappears (Fig. 10). The resulting freshwater front (e.g., as hinted by 30 g/kg isohaline) differs from that in 2012 as well, having retreated to the southern latitudes. Under this scenario, the temperatures at the bottom layers remain identical to those of 2013, but the surface layer becomes slightly colder. The latter is explained by the increasing stability of the water column due to the extra buoyancy caused by the flood event in 2013, reflected by the larger area of intense (>1 kg m^{-3}) density stratification (Fig. 11, compare 2013 and 2013-R12).

https://doi.org/10.5194/bg-2020-1
Preprint. Discussion started: 31 January 2020

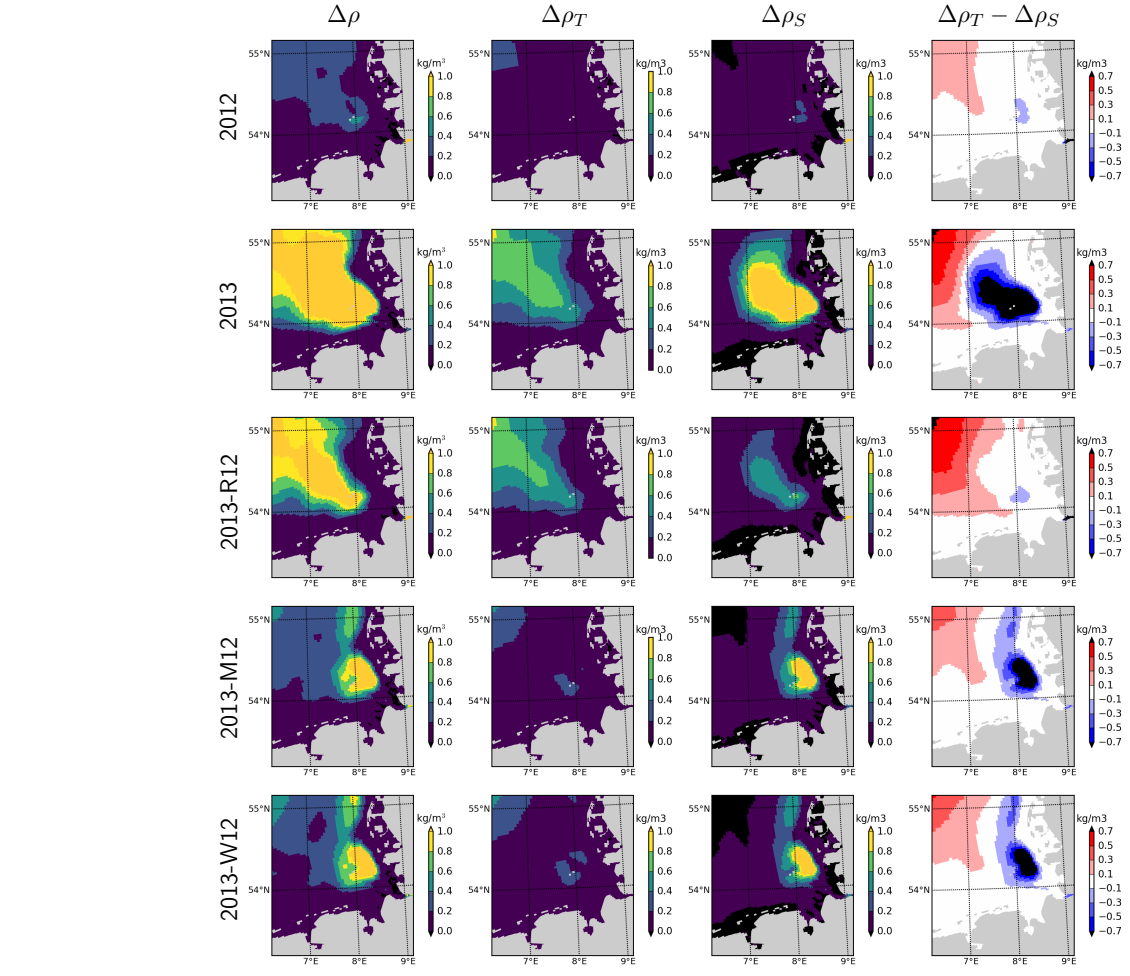

Figure 11. Density difference between the surface and bottom layers ($\Delta\rho$), contribution of temperature and salinity, $\Delta\rho_T$ and $\Delta\rho_S$ (as estimated by the linearized equation of state: $\rho - \rho_0 = \alpha(T - T_0) + \beta(S - S_0) + \gamma(P - P_0)$, with α = -0.15 kg m^{-3}/K and β = 0.78 kg m^{-3} / (g kg $^{-1}$)), and their difference ($\Delta\rho_T$ - $\Delta\rho_S$), during July for the years 2012 and 2013 and scenarios 2013-R12, 2013-M12 and 2013-W12.

Effect of exchanging the entire meteorological conditions (as indicated by the 2013-M12 scenario), and only that of the short-term (i.e., starting from June) wind forcing (2013-W12 scenario) on the salinity distribution is almost identical: according to both scenarios, the freshwater plume around the mouth of Elbe and Weser is preserved, but the plume spreads along the coast instead of spreading towards the outer German Bight as was the case in the original 2013 simulation (Fig. 10). Thus, the distribution of salinity within the central and outer German Bight in July 2013 can concluded to be driven by the short-term wind conditions. The freshwater front (e.g., as indicated by the 27-30 g/kg isohalines) simulated according to both 2013-M12 and 2013-W12 scenarios extend further to North in comparison to 2012, which is evidently driven by the additional freshwater inputs due to the flood.

https://doi.org/10.5194/bg-2020-1
Preprint. Discussion started: 31 January 2020

Temperatures simulated according to 2013-M12 scenario are similar to those simulated for 2012, characterized by relatively low temperatures at the surface and the relatively high temperatures at the bottom, in comparison to the original estimations for 2013. Interestingly, the temperatures simulated by the 2013-W12 scenario are similar to those simulated by the 2013-M12 scenario, indicating that the large differences in surface and bottom temperatures during July 2013 was mainly caused by the wind conditions. In the 2013-W12 scenario, enhanced turbulent vertical mixing driven by the stronger winds of the July 2012 does not allow the surface temperatures to build up, while it causes the cold bottom temperatures to increase to the levels originally simulated for July 2012, except within the northeastern margin of the study region, where the bottom temperatures remain cold.

The combination of temperature and salinity dynamics determines the 3-dimensional density (ρ) structure of the system. The difference between the density of the surface and bottom layers ($\Delta\rho$) therefore indicates the intensity of the thermohaline stratification, and hence, gives insight into the average light conditions primary producers experience in the deeper zones. Average $\Delta\rho$ during July 2012 indicate a weak stratification in the outer German Bight with values mostly below 0.4 kg m^{-3}, with the exception of a small patch south of Helgoland (Fig. 11). During July 2013, $\Delta\rho$ displays an area of strong stratification ($\Delta\rho >$ 1.0 kg m^{-3}) penetrating to the inner German Bight along the old Elbe Valley. Contributions of temperature and salinity to the $\Delta\rho$, i.e., $\Delta\rho_T$ and $\Delta\rho_S$, suggests that $\Delta\rho_S$ is larger than $\Delta\rho_T$ in a region surrounding and extending northwest of Helgoland. The 2013-R12 scenario results in a $\Delta\rho$ similar in intensity and shape to that in 2013, only narrower in the inner German Bight, whereas the $\Delta\rho$ estimated by the 2013-M12 and 2013-W12 scenarios are small within the outer areas as in 2012, but forms a strong patch located northeast of Helgoland.

Simulated DISi and DIN plumes of Elbe in 2013 July following the flood event (Fig. 12) resemble the freshwater plumes (Fig. 10). This plume disappears when the river forcing of the 2012 is used (2013-R12) and it gets pushed along the eastern coast in the 2013-M12 scenario (Fig. 12), similar to the freshwater plume (Fig. 10). The plume of the DIP on the other hand, when scaled to the Redfield proportions (molar N:P=16), is confined to a smaller region closer to the Elbe estuary. Thus, the impact of the river plume on the nutrients can be tracked by the enhanced N:P ratios.

Spatial distribution of the water-column integrated net primary production rate, NPPR is considerably different in July 2013 than in July 2012 (Fig. 12). Two areas with prominent changes can be distinguished: *i)* outer German Bight (OGB), i.e., west of 7.5 °E and north of 54.5 °N; *ii)* central German Bight (CGB), i.e., region around Helgoland, and its westward and northward extensions. Within the OGB, NPPR estimated for 2013 is lower than 2012 and by 2013-M12/W12. This can be explained by the nutrient limited phytoplankton growth in this region, and the intensification of nutrient limitation due to stronger stratification in 2013 driven by meteorological conditions (Fig. 11). Within the CGB, the distinctive patch of high NPPR that is narrowly present in July 2012 expands considerably in July 2013. In comparison to 2013, the 2013-R12 scenario results in a weakening of NPPR within the entire CGB, in terms of both peak rates and areal coverage of high values, especially in the northern portion. The 2013-M12/W12 scenarios also lead to local reductions of the peak rates achieved at around and north of Helgoland, pointing to the relevance of the hydrological conditions for the intensity of NPPR during July 2013. The enhancement of NPPR within the CGB can be explained by the enhancement of light conditions due to strong stratification in this nutrient-rich region, especially following the flood event (Fig. 12).

https://doi.org/10.5194/bg-2020-1
Preprint. Discussion started: 31 January 2020

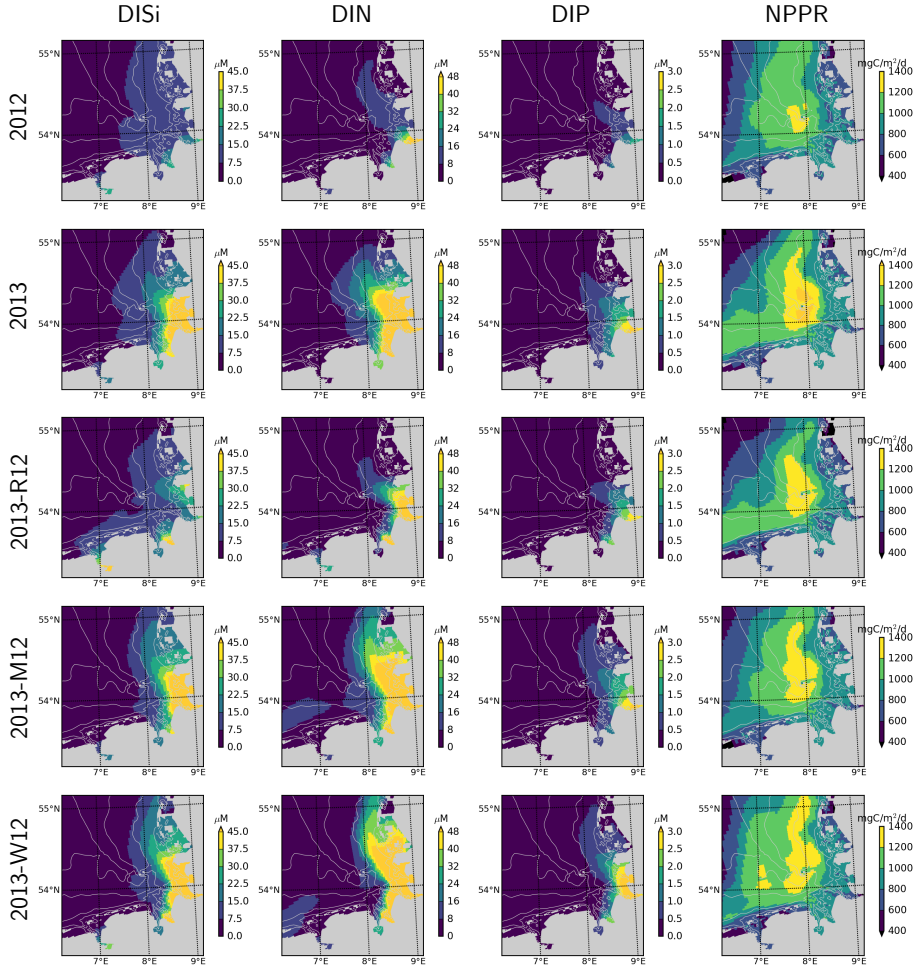

Figure 12. Surface DISi, DIN, DIP and integrated net primary production rate during July for the years 2012 and 2013 and scenarios 2013-R12, 2013-M12 and 2013-W12.

In 2012, the DO remains close to the saturation. Contrastingly, in July 2013, a widespread patch of oxygen subsaturation (< 90% of saturation) develops within the bottom layers of the CGB, which further intensifies (< 80%) and expands towards the OGB during August 2013. Occurrence of this oxygen subsaturation can be explained by the enhanced dissolved oxygen (DO) consumption fueled by the increased NPPR within the CGB (Fig. 12) and the intense stratification within the entire German Bight (Fig. 11) that limits the oxygenation of the bottom layers. In the OGB, occurrence of the oxygen subsaturation despite the lower NPPR (Fig. 12) highlights the relevance of stratification (Fig. 11). Under the 2013-R12 scenario, the oxygen levels do not drop as much as in the 2013 scenario within the CGB, and the area with oxygen subsaturation becomes narrower especially during July, but also in August. The 2013-M12 and 2013-W12 scenarios result in a complete disappearance of the oxygen subsaturation within the CGB during July, pointing to the effectiveness of wind-induced mixing in the oxygenation of bottom

https://doi.org/10.5194/bg-2020-1
Preprint. Discussion started: 31 January 2020

Biogeosciences Discussions Open Access EGU

layers. Within the OGB, oxygen falls below sub-saturation levels in August according to the 2013-W12 scenario, that can be explained by the thermal stratification obtained in this region with this scenario (Fig. 11).

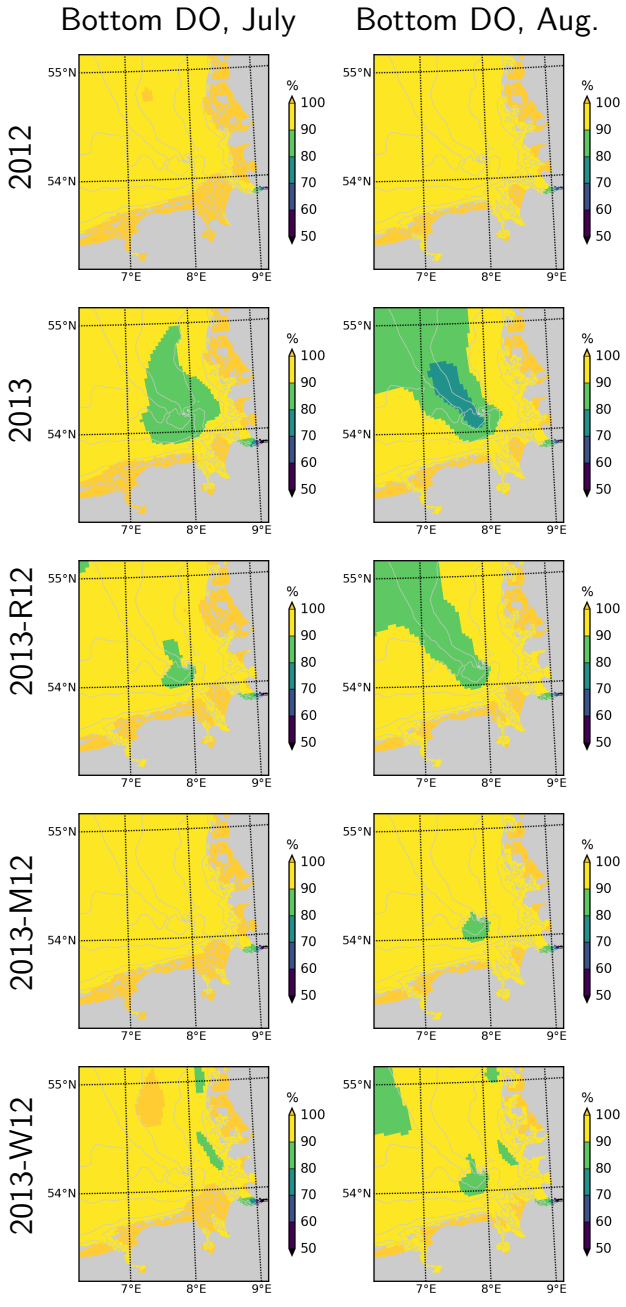

Figure 13. Dissolved oxygen in bottom layers during July and August, for the years 2012 and 2013 and scenarios 2013-R12, 2013-M12 and 2013-W12.

https://doi.org/10.5194/bg-2020-1
Preprint. Discussion started: 31 January 2020

At the Deutsche Bucht station, where the temperature and salinity measurements were shown to be reasonably reproduced (Fig. 6), the DO measurements are also mostly well reproduced (Fig. 14). Importantly, the higher levels of supersaturation during 2013 in comparison to 2012, driven by higher NPPR (Fig. 12), and the oxygen depletion in the bottom layers in 2013, and the lack thereof in 2012 are qualitatively reproduced. Especially the 2013-M12/W12, and to a lesser extent, 2013-R12 scenarios result in lower levels of supersaturation at the surface, indicating lower levels of NPPR (Fig. 12). At the bottom, especially the 2013-M12/W12 scenarios result in the disappearance of the oxygen drawdown in July 2013, which is driven by both lesser amounts of organic material to degrade as a result of lower NPPR, and the oxygenation of bottom layers via vertical mixing caused by the windy conditions of 2012. The 2013-R12 results in a lower level of drawdown in comparison to the reference (2013) simulation, and an earlier recovery back to the saturation levels.

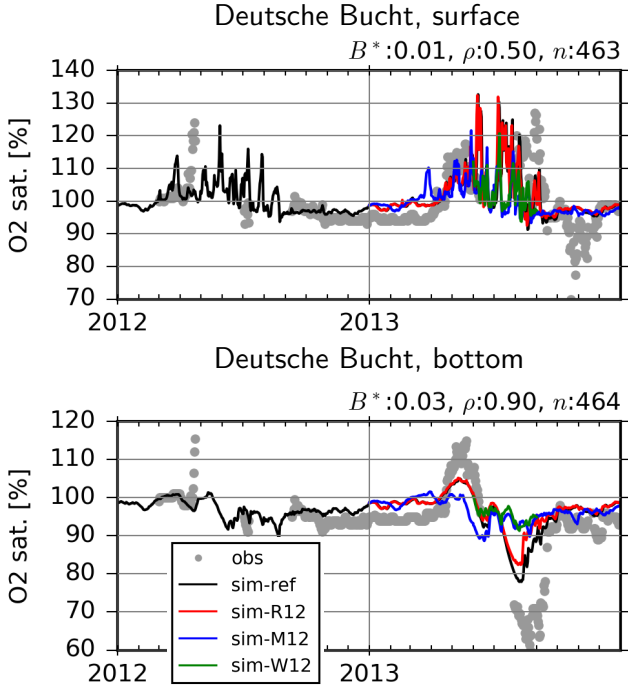

Figure 14. Oberved (dots) and simulated (lines) dissolved oxygen in the surface and bottom layer at the Deutsche Bucht station. $B*$: normalized bias, ρ: correlation coefficient, n: number of observation-simulation pairs based on the reference (ref) run.

In order to demonstrate the effects of thermohaline structure on the current velocities, we consider two specific days characterized by different wind regimes in June 2013, and compare the original estimates with those obtained with 2013-R12 scenario (Fig.15). In order to remove the movements caused by lunar (M2) tides, the current velocities with 30 min. resolution were averaged over 25h intervals, centered around 12:00 of each day. Differences between the two simulations (Fig.15b,e) reveal an increase in current velocities at the surface within the zone affected by the river plume. At the bottom layers, differences occur as well, but these are smaller in magnitude (not shown).

https://doi.org/10.5194/bg-2020-1
Preprint. Discussion started: 31 January 2020

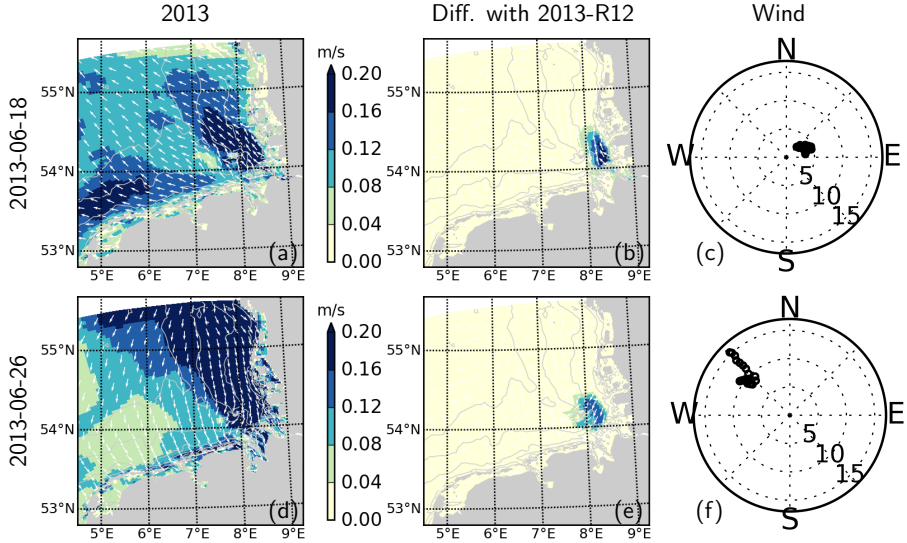

Figure 15. 25h-averaged (residual) current velocities at the surface (a,d) and the difference with those obtained with 2013-R12, during two different wind conditions (c,f). In panels c,f, wind speed at each hour within the day is marked, with distance from origin indicating wind speed, in m/s.

For a better understanding of the modulation of the flow structure by the flood event within the coastal zone, we elaborate 3 cross-shore transects, two of which cross through the monitoring stations, nutrient concentrations at which were displayed in Fig. 9), and for 18 June 2013 that was considered in Fig. 15e-h, regarding the surface current velocities. On this particular day, an estuarine-like circulation is strongly manifested along the southern part of the north-Frisian Wadden Sea (see Fig. 1), with the cross-shore (x-) velocities at the bottom layers directed towards the shore, and at the surface directed off the shore (Fig.16). Removal of the flood event, as predicted by the 2013-R12 results in a weakening of the bottom currents at the southern section (as represented by Suederpiep) and the middle section (as represented by Westerhever). The along-shore (y-) velocities at the bottom layers, directed towards south (outwards the plane) display a similar weakening of the bottom currents. These results indicate that the efficiency of estuarine circulation is determined by an interplay between the meteorological and hydrological conditions.

https://doi.org/10.5194/bg-2020-1
Preprint. Discussion started: 31 January 2020

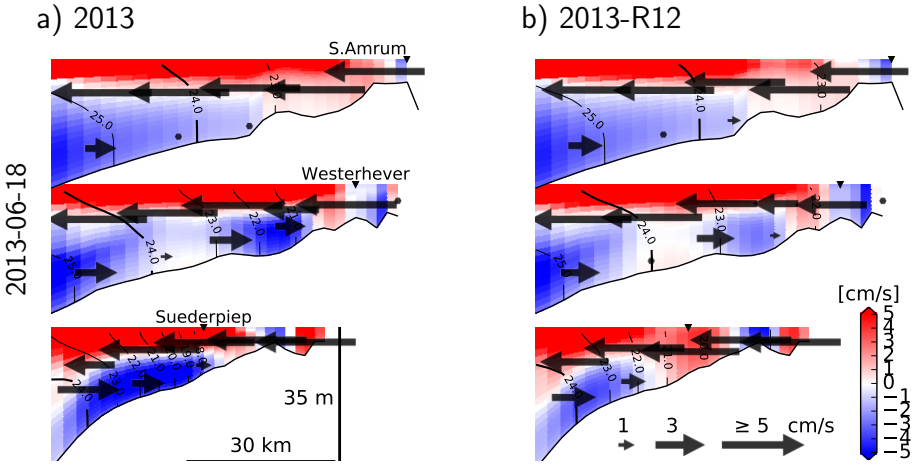

Figure 16. 25h-averaged velocity and density structure simulated with the reference model (a) and with the riverine forcing of 2012 (b), under the northeasterly winds on June 18, 2013 (see Fig.15). Two of the transects cross from the stations shown in Fig.9 (marked by ▼ symbols). Arrows indicate the cross-shore velocities, and the colors indicate along-shore velocities with positive values indicating northward flows (i.e., inward the drawing plane). Contour lines indicate σ_T.

4 Discussion

4.1 Model Performance

In comparison to the performance of the previous version of the hydrodynamical model setup presented by Kerimoglu et al. (2017a), the ability of the model in representing the cross-shore salinity gradients has been significantly improved, mainly due to the introduction of flow-dependent horizontal diffusion (e.g., Fig.A1). As suggested by the comparisons with ICES data (Fig. 5), realism of temperature has also been improved, with the normalized bias decreasing from -0.11 to -0.03, and the correlation increasing from 0.95 to 0.99 (compare with Fig. 4 of Kerimoglu et al. (2017a)). There have been incremental improvements in the prediction of nutrient concentrations as well. However, these minor deviations may be related with the differences in specific time periods of interest (2006-2010 in the former study vs 2011-2014 in this study).

The underestimation of salinities (Fig. 7), and consequently the overestimation of nutrient concentrations along the coast (Fig.9) are possibly related with the underestimated flushing rate at the coastal zone. Before the application of explicit horizontal diffusion, these errors were much larger (Appendix A). Application of higher horizontal diffusion rates (e.g., via higher Smagorinsky coefficient C_S, see Appendix A) further improved the model performance along the east Frisian Wadden Sea, however, at the cost of overestimation of salinities at the mouth of the estuary, such as at the Cuxhaven station (Fig.6); as well as further dampening of the tidal amplitudes, which are already slightly underestimated (not shown). A spatially variable C_S field, with gradually decreasing values at the mouth of the Elbe helped circumventing this problem, but this spatially variable parameterization was not adopted in this study. Before resorting to such ad-hoc solutions, other potential sources of error needs to be assessed.

https://doi.org/10.5194/bg-2020-1
Preprint. Discussion started: 31 January 2020

A potential source of bias in salinity and nutrients along the Elbe-plume is the misrepresentation of the Elbe estuary in our model setup (Fig. 1). For instance, according to a recent, high resolution model of the Elbe estuary, the freshwater-saline water transition (0-5 g/kg) occurs at about 50-75 km upstream of the mouth of Elbe (under normal hydrological conditions), and the N and Si concentrations vary considerably within the estuary (Pein et al., 2019). Indeed, a high resolution (300m) setup of the German Bight that resolves up to 150 km upstream the Elbe mouth (Chegini et al., submitted) demonstrated better skill in reproducing the salinity observations shown in Fig.7 and Fig. A1. Another contingent error source is potential inaccuracies in advective transport rates, e.g., as a result of imperfections in meteorological forcing (Geyer, 2014) or ignoring the effects of off-shore wind-farms on the thermohaline circulation (Carpenter et al., 2016; Platis et al., 2018). In order to assess the realism of the advective transport rates estimated by our hydrodynamic setup, we are planning to do a comparison with other models, such as the operational model of the BSH (see Callies et al., 2017).

Despite these limitations, the model was able to reproduce various characteristic features of the system, as indicated by low bias and high correlation coefficients in general (e.g., Fig. 5). Importantly, the influence of the meteorological and hydrological peculiarities on the hydrodynamical (Figs. 6, 7, A1) and biogeochemical structure of the system were captured (Figs.8, 9, 14). The skill of the model at the Helgoland station, both with respect to the physical (Fig.6) and biogeochemical variables (Fig.8) is notable, given the heterogeneities caused by the complex topography, and the sharp gradients around the island (Callies and Scharfe, 2015). We conclude that the model can be used for an exploratory analysis to gain a better understanding of the role of riverine and meteorological forcing in shaping of the hydrodynamical and biogeochemical structure of the German Bight.

Since the first 3D models of the North Sea (Backhaus, 1985; Dippner, 1993; Schrum, 1997), computational capacity has been significantly improved, which resulted in development of ever finer resolution setups that can resolve meso-scale features such as the coastal freshwater fronts and baroclinic eddies (Holt and James, 2006; Pohlmann, 2006; Staneva et al., 2009; Pätsch et al., 2017) and the smaller-scale dynamics, such as the estuarine mixing (Gräwe et al., 2016; Stanev et al., 2019). For large-domain biogeochemical applications that require a costly calculation of transport of dozens of additional state variables, the coarse-resolution models (10-20 km) are being actively used (e.g., Ford et al., 2017; Große et al., 2016; Daewel et al., 2019). With a spatial resolution of 1.5-4.5 km covering the southern North Sea (Fig. 1), the setup we employed here falls somewhere in the middle of the spectrum, and is similar to the setup used by Los et al. (2008) and the 'southeastern North Sea' setup of Androsov et al. (2019). Based on a 144-node setup on the Mistral-phase 2 HPC environment (https://www.dkrz.de/en-pdfs/en-docs/en-docu-mistral/en-mistral_user-manual.pdf), computational cost of the full, coupled model system (i.e., with the biogeochemical model with 25 pelagic state variables, Fig.2) is about 360 CPUh/year (approximate speed-up (simulated time interval over duration of simulation) of 3500), while that of the uncoupled physical model is about 80 CPUh/year (approximate speed-up of 16000). Thus, the setup is suitable for performing coupled physical-biogeochemical simulations or scenario analyses with multi-annual or even decadal time scales.

4.2 Physical and biogeochemical structure of the system

Based on a plethora of *in-situ* observations, Voynova et al. (2017) reported a number of anomalies in the German Bight, following the historical flood event in June 2013, during which, a large quantity of freshwater and nutrients were delivered by

https://doi.org/10.5194/bg-2020-1
Preprint. Discussion started: 31 January 2020

the Elbe and Weser rivers within a short time period (Fig. 3). Our numerical simulations are in agreement with many of those findings, such as the anomalous spatial distribution of salinity, nitrogen and silicate following the flood event (e.g., compare Fig. 10, 12 with the Fig. 11 of Voynova et al. (2017)).

In addition, our findings point to the relevance of the meteorological conditions that interact with the impacts of the flood event. In particular, our findings suggest that mainly the wind conditions (Fig. 4) resulted in a particularly intense stratification (Fig.11). Within the central German Bight, a combination of thermal and haline dynamics extended the area of intense stratification. The thermohaline dynamics in the inner German Bight have been recognized before (Frey, 1990; van Leeuwen et al., 2015). Following the flood event, these interactions have moved away from the coast to further offshore regions of the German Bight. It should be noted that, variations in stratification intensity driven by the spring and neap tides as in the Rhine ROFI (Simpson et al., 1993) have been identified for our study system as well, but these are relevant at shorter (weekly) time scales (Chegini et al., submitted).

The enhanced water column stability (Fig. 11), and hence reduced light limitation, in combination with higher nutrient availability supplied by the flood event (Fig. 3, 12) increased the NPPR within the central German Bight (Fig. 12), which may explain the high pH and DO oversaturation reported by Voynova et al. (2017). In turn, the combination of prolonged stratification (Fig. 11) and the breakdown of high amounts of organic material as a result of enhanced NPPR (Fig. 12) following the flood event lead to a widespread oxygen depletion. The DO supersaturation at the surface and bottom layers, and subsequent subsaturation in bottom waters observed in the Deutsche Bucht station, which was previously documented by Voynova et al. (2017), was correctly captured by the model (Fig.14). The scenario analysis suggests that especially the meteorological conditions during the summer of 2013, but also the flood event were relevant for the occurrence and intensity of this oxygen drawdown in the German Bight (Fig. 13-14). This explains why such a degree of oxygen depletion in the German Bight is unusual (e.g., Voynova et al., 2017; Große et al., 2016, 2017). Within the outer German Bight, the higher water column stability lead to an intensification of the nutrient limitation within the upper mixed layer, and consequently lower NPPR (Fig. 12). At the vicinity of the mouth of Elbe-Weser rivers, NPPR does not respond strongly to the flood (Fig. 12), as these areas are more limited by light, than nutrients (see also Loebl et al., 2009). In reality, an even stronger light limitation in the vicinity of the mouth of the Elbe estuary is likely, due to the increase in the SPM towards the Elbe estuary (van Beusekom and Brockmann, 1998; Gayer et al., 2006), which is only partially accounted for by the model (see Appendix B2). It should be noted that the riverine influence within the coastal zone may be overestimated by our simulations, given the lower than observed salinities (Fig. 7), higher than observed nutrient concentrations (Fig. 9).

Our results point to an increase in current velocities at the surface under the influence of the 2013 flood (Fig. 15), which is presumably driven by the reduced dissipation of kinetic energy through vertical mixing, owed to the intensification of haline stratification (Fig. 11), i.e., the baroclinicity of the current structure. Enhancement of the current velocities at the surface, in turn, might have facilitated the spread of the plume towards the outer German Bight in 2013 (Fig.10-12). However, the main reason for the eastward spread of the plume is the wind conditions, which presumably lead to a dominance of anticyclonic circulation during July 2013, as also suggested by a principal component analysis of a barotropic model simulation (https://coastmap.hzg.de/coastmap/modeldata/model1/#/residualcurrents, see Callies et al. (2016) for data access). It has been earlier

https://doi.org/10.5194/bg-2020-1
Preprint. Discussion started: 31 January 2020

shown that the residual surface currents in the German Bight are largely determined by the wind patterns (Schrum, 1997; Callies et al., 2017).

van Beusekom et al. (2019) had earlier showed and discussed the presence regional differences in thermohaline estuary-type circulation (as in Burchard and Badewien, 2015; Hofmeister et al., 2017) in the Wadden Sea. Here, our results suggest that the strength of the thermohaline estuarine circulation (Burchard and Badewien, 2015) can be enhanced by surplus buoyancy fluxes, here driven by the flood event (Fig. 16), which is as expected and can enhance coastal accumulation of SPM and nutrients even distant to the estuary itself (Hofmeister et al., 2017).

Our model-based analysis here is not conclusive, but rather exploratory. Given the anticipated increase in the frequency and intensity of the hydro-meteorological extremes due to climate change (Beniston et al., 2007; Wetz and Yoskowitz, 2013), further research is needed to understand the processes underlying the interactive impacts of these events on the physical and biogeochemical structure of the coastal systems and estuaries. Such a mechanistic understanding is essential for policy making, such as the regulation of nutrient loading rates in rivers (see, e.g., OSPAR, 2017).

5 Conclusions

In this study, we presented a newly developed biogeochemical model and improvements of a hydrodynamical model described in an earlier study. The coupled hydrodynamical-biogeochemical model system is shown to satisfactorily reproduce the characteristic features of the German Bight ecosystem, and the impacts of a 100-year flooding of the Elbe and Weser rivers. Our results reveal that the flood event coincided with special meteorological conditions in the region, namely a calm and warm summer dominated by an anticyclonic circulation, resulting in a particularly intense and widespread stratification. The stronger stratification, and the increased availability of nutrients impacted the primary production in the system and the oxygen levels at the bottom waters. Through a scenario analysis, we found out that the observed anomalies in July 2013 were likely driven by both the meteorological conditions within the outer German Bight, and their interaction within the central German Bight, suggesting that the impacts of the flood events in the system are context-dependent. These conditions may occur more frequently in the future, which requires a better understanding of the mechanisms governing the response of the coastal systems to such extreme events.

Code and data availability. Codes of the hydrodynamical models and the coupler are available at the following git repositories: GETM: https://sourceforge.net/p/getm, GOTM: https://github.com/gotm-model, FABM: https://github.com/fabm-model/fabm. The biogeochemical model code will be released in the near future, but a beta version can be provided by OK upon request. ICES and COSYNA data used for model validation are available from https://ices.dk and https://cosyna.de, respectively. Data from Terschelling and Noordwijk stations are available at https://waterinfo.rws.nl. Surface elevation, meteorological and EMEP atmospheric deposition data used as model forcing are available from, respectively: https://doi.org/10.1594/WDCC/coastDat-2_TRIM-NP-2d, https://doi.org/10.1594/WDCC/coastDat-2_COSMO-CLM and https://emep.int. EMODnet bathymetry data is available from https://emodnet-bathymetry.eu. Model output of the current study will be provided by OK upon request.

https://doi.org/10.5194/bg-2020-1
Preprint. Discussion started: 31 January 2020

Biogeosciences Discussions Open Access EGU

Appendix A: Description of horizontal diffusion in the hydrodynamical model

Modern advection schemes (including TVD-transport as used in many coastal applications) are developed and tested for homogeneous grid spacing (Pietrzak, 1998; Barthel et al., 2012), although coastal applications tend to use varying grid spacing in curvilinear horizontal, unstructured horizontal and general vertical grids (e.g., Zhang et al., 2016; Kerimoglu et al., 2017a). The performance of slope limiters and the involved numerical mixing is therefore almost unpredictable for two reasons: a) tracer mixing is ultimately always a combination of numerical mixing and physical mixing terms, both effects reduce each other (Hofmeister et al., 2011), and b) numerical mixing as a nonlinear effect of the advection is seldom analyzed in model applications. Comparisons of the mixing term strength between model applications then potentially result in differences of the advection scheme performance, more than an analysis of the physical effect of mixing mass concentrations.

There exists a plethora of methods for the specification of horizontal diffusion or isopycnal mixing for ocean models (see, e.g. Gent and McWilliams, 1990; Roberts and Marshall, 1998; Beckers et al., 2000; Griffies and Hallberg, 2000), a review or discussion of which is beyond the scope of this appendix. Here, we will demonstrate the use of a simple subgridscale parameterization by Smagorinsky (1963), which was originally for modelling atmospheric circulation, and is now commonly used in both atmospheric and ocean circulation models (Becker and Burkhardt, 2007). The magnitude of horizontal diffusivity is recognized to exhibit strong variations in space and time (Wang, 2003). The Smagorinsky parameterization achieves such variations by scaling the diffusion coefficient proportionally with the grid size and deformation rates of lateral velocities, e.g., for the horizontal diffusion of momentum:

$$A_M = C_S * \Delta x \Delta y * \sqrt{\left(\frac{\partial u}{\partial x}\right)^2 + \left(\frac{\partial v}{\partial y}\right)^2 + \frac{1}{2}\left(\frac{\partial u}{\partial y} + \frac{\partial v}{\partial x}\right)^2} \tag{A1}$$

where, C_S is the empirical Smagorinsky constant, u, v, Δx and Δy are velocities and grid spacings along x and y dimensions, respectively. Then the horizontal diffusion of tracers, A_H follows:

$$A_H = A_M / Prt \tag{A2}$$

In (A1), C_S is not physically well constraint, but is adjusted based on numerical considerations (Kantha and Clayson, 2000), e.g., the diffusion vs. dispersion trade-off (Pietrzak, 1998). In this study, we set $C_S = 0.6$ and Prandtl number, $Prt = 1.0$, and examine the effects of this parameterization on the representation of the river plume during 2012-2013, with a focus on the freshwater plume during the flooding event. Specifically, we compare the predictions of 2 model variants against the Ferrybox measurements taken by the platform installed on the M/V *Funny Girl* ferry, that are analyzed in greater detail in the main text (Fig. 7).

The variant where no diffusion was enabled, overestimates the cross-shore salinity gradient along the North Frisian coast, i.e., North of Elbe, in the form of too low near-coast salinities (Fig.A1b). On the other hand, the variant where horizontal diffusion was described with Smagorinsky parameterization, have considerably better skill in reproducing the FerryBox measurements along the Büsum-Helgoland ferry track (Fig. A1c).

https://doi.org/10.5194/bg-2020-1
Preprint. Discussion started: 31 January 2020

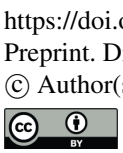

Biogeosciences Discussions
Open Access
EGU

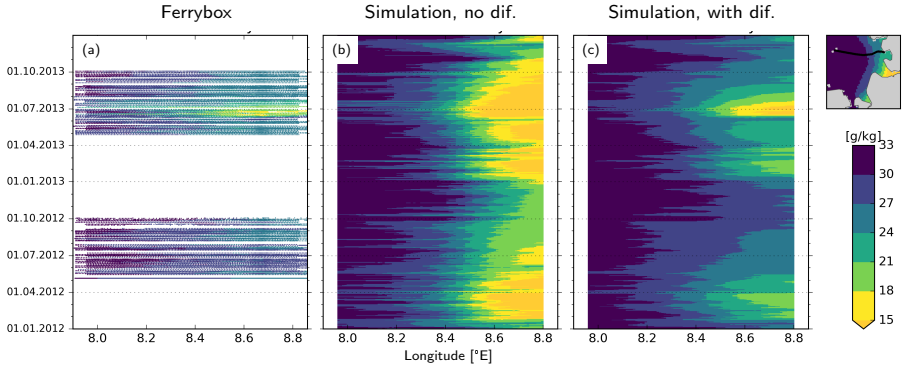

Figure A1. Hovmöller diagrams of salinity distribution in 2012 and 2013 along the (average) transect shown at the top right corner, as measured by the FerryBox platform (a) and models without (b) and with (c) horizontal diffusion.

Plausibility of the total horizontal mixing, and its physical and numerical components can be diagnosed by an analysis of the discrete variance decay (DVD) of salinity (Klingbeil et al., 2014) based on Burchard and Rennau (2008). In the absence of explicit diffusion, the sum of physical and numerical mixing becomes negative at the mouth of the Elbe and Weser rivers, and within their ROFI, implying spuriously enhanced horizontal gradients (Fig. A2c). With the application of explicit diffusion, numerical mixing values effectively decrease both within the positive and negative spectra (Fig. A2d), leading to near-complete elimination of negative values of the total mixing being removed (Fig. A2f).

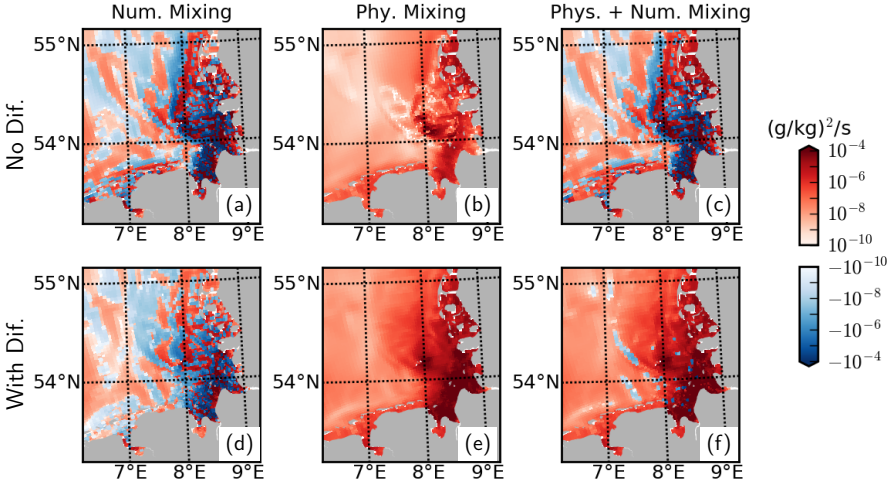

Figure A2. Mixing analysis for July 2013 based on temporally averaged values at the surface.

We conclude that application of explicit horizontal mixing through a simple parameterization can be useful in improving the skill of a 3-D coupled physical-biogeochemical model within the vicinity of river discharges, and eliminate implausible negative total (physical + numerical) mixing values.

https://doi.org/10.5194/bg-2020-1
Preprint. Discussion started: 31 January 2020

Appendix B: Detailed description of the biogeochemical model

All modelled state variables and fluxes between various pools are shown in Fig. 2. In the following sections, sink and source terms for the planktonic and abiotic variables ($s(v)$ in Tables B1, B7) and the description of processes (Tables B2, B4, B9) will be provided. For describing the fluxes between various pools, where possible, we adopt the $source\_target$ notation as in Pätsch and Kühn (2008). Although this notation is consistent with that used in the Fortran program of abiotic components, the programming notation of the Planktonic components are somewhat different, due to their different historical origins.

All kinetic rates in planktonic and abiotic components are modified with temperature using the Q10 rule:

$$f_{T,(phy,zoo-j,abio)} = Q10^{(T-T_{ref})/T_{ref}}_{(phy,zoo-j,abio)} \tag{B1}$$

with $T_{ref} = 10°\text{C}$, and $Q10_{phy} = Q10_{zoo-mic} = Q10_{abio} = 1.5$ and $Q10_{zoo-mes} = 2.0$.

B1 Planktonic components

The plankton model was developed based on Kerimoglu et al. (2017b) regarding the modularity concept that allows coupling plankton units in run time (see Bruggeman and Bolding, 2014), as well as description of internal variation of P quota of phytoplankton (B2,B4,B12) according to the Droop model (as in Morel, 1987). Here, we further considered the uptake NO3 and NH4 of phytoplankton (similar to Pätsch and Kühn, 2008), and the resulting variations of N quota (B3,B13); limitation of diatoms by Si (B11) using a Monod-type relationship (Flynn, 2003); dependence of the light limitation on the chlorophyll content, i.e., θ (B15), in phytoplankton (B9), and the dynamic variations of θ (B5,B16) following Geider et al. (1997).

Table B1. Source-sink terms of the dynamic variables (all in mmol/m^3/d) of the plankton module. Indices p_i= {diatoms, nanoflagellates}; z_j={microzooplankton,mesozooplankton}; t_k= zooplankton target.

C bound to p_i	$s(p_i^C)$	$= DIC\_p_i^C - p_i^C\_DOC - M_i^C - \sum_j I_{j,i}^C \cdot z_j^C$	(B2)
N bound to p_i	$s(p_i^N)$	$= NO3\_p_i^N + NH4\_p_i^N - p_i^N\_DON - M_i^N - \sum_j I_{j,i}^N \cdot z_j^C$	(B3)
P bound to p_i	$s(p_i^P)$	$= DIP\_p_i^P - p_i^P\_DOP - M_i^P - \sum_j I_{j,i}^P \cdot z_j^C$	(B4)
Chl bound to p_i	$s(p_i^{chl})$	$= \rho_i \cdot DIC\_p_i^C - (p_i^C\_DOC + M_i^C + \sum_j I_{j,i}^C \cdot \theta_i \cdot 12.0[gC/molC] \cdot z_j^C$	(B5)
C bound to z_j	$s(z_j^C)$	$= \sum_k t_k^C\_z_j^C - zC_j\_DIC - M_j^C$	(B6)

As in Kerimoglu et al. (2017a), sinking rate of phytoplankton is formulated as a function of their nutrient status.

$$w_{p,i} = w'_p \cdot \left(0.1 + 0.9 \cdot \exp\left(-5.0 * \min\left(\frac{QP_i - QP_{min,i}}{QP_{max,i} - QP_{min,i}}, \frac{QN_i - QN_{min,i}}{QN_{max,i} - QN_{min,i}}\right)\right)\right) \tag{B7}$$

In (B7) and in Tables B1-B2, $QX = X:C$ within a certain phytoplankton or zooplankton pool, which may be either a fixed constant (as provided in Table B3), or diagnostically calculated from the instantaneous values (for $X = P, N$ quota of phytoplankton). Exudates of the phytoplankton are assumed to be in DOM form (B2,B17).

https://doi.org/10.5194/bg-2020-1
Preprint. Discussion started: 31 January 2020

Table B2. Process equations and functional relationships used in the phytoplankton module

C uptake rate of p_i	$DIC\_p_i^C$	$= p_i^C \cdot f_{T,phy} \cdot V_{max,i}^C \cdot f_{I,i} \cdot \min(f_{N,i}, f_{P,i}, f_{Si,i})$	(B8)
Light limitation of p_i	$f_{I,i}$	$= 1.0 - \exp\left(\frac{-\alpha_i \cdot \theta_i \cdot I}{f_{T,phy} \cdot V_{max,i}^{C \cdot \min(f_{N,i}, f_{P,i})}}\right)$	(B9)
Nutrient (X={N,P}) limitation of p_i	$f_{X,i}$	$= 1.0 - QX_{min,i}/QX_i$	(B10)
Silicate limitation of diatoms	$f_{Si,i}$	if $i : diatoms$ $= \frac{DISi}{K_i^{Si}+DISi}$, else $= 1.0$	(B11)
DIP uptake rate of p_i	$DIP\_p_i^P$	$= p_i^C \cdot f_{T,phy} \cdot V_{max,i}^P \cdot \frac{QP_{max,i}-QP_i}{QP_{max,i}-QP_{min,i}} \cdot \frac{DIP}{K_i^P+DIPi}$	(B12)
DINX (NX={NO3,NH4}) uptake rate of p_i	$DIX\_p_i^N$	$= p_i^C \cdot f_{T,phy} \cdot V_{max,i}^N \cdot \frac{QN_{max,i}-QN_i}{QN_{max,i}-QN_{min,i}} \cdot \frac{DINX/K_i^{NX}}{1.0+\sum_X DINX/K_i^{NX}}$	(B13)
Silicate uptake rate of p_i	$DISi\_p_i^{Si}$	if $i : diatoms$ $= DIC\_p_i^C \cdot QSi_i$, else $= 0.0$	(B14)
Chl:C ratio bound to p_i	θ_i	$= p_i^{chl}/(p_i^C \cdot 12$[gC/molC])	(B15)
Ratio of chl. synthesis to C fixation	ρ_i	$= \frac{DIC\_p_i^C/p_i^C}{\alpha_i \cdot \theta_i \cdot I}$	(B16)
X (=C,N,P) exudation of p_i	$p_i^X\_DOX$	$= DIC\_p_i^C \cdot \gamma_i \cdot QX_i$	(B17)
X (=C,N,P) Mortality rate of p_i	M_i^X	$= p_i^X \cdot f_{T,phy} \cdot (m1_i + p_i^C \cdot m2_i)$	(B18)

Table B3. Parameters of the phytoplankton module. Where necessary, multiple values were provided for diatoms and nanoflagellates.

Symbol	Description	Value$_i$	Unit
$V_{\text{max,i}}^C$	Maximum C uptake rate	3.0,2.0	d^{-1}
$V_{\text{max,i}}^N$	Maximum N uptake rate	0.3,0.6	molN (mmolC d)$^{-1}$
$V_{\text{max,i}}^P$	Maximum P uptake rate	0.01,0.02	molP (mmolC d)$^{-1}$
K_i^{NO3}	Half saturation constant for NO3 uptake	3.0	mmolN m^{-3}
K_i^{NH4}	Half saturation constant for NH4 uptake	1.0	mmolN m^{-3}
K_i^P	Half saturation constant for P uptake	0.4	mmolP m^{-3}
K_i^{Si}	Half saturation constant for Si limitation	1.0	mmolSi m^{-3}
Q^Si_{diat}	Fixed Si:C ratio of diatoms	0.17,0.0	molSi $molC^{-1}$
$QN_{\text{max,i}}$	Maximum quota for N	0.18	molN $molC^{-1}$
$QP_{\text{max,i}}$	Maximum quota for P	0.008	molP $molC^{-1}$
$QN_{min,i}$	Subsistence N quota	0.045,0.06	molN $molC^{-1}$
$QP_{min,i}$	Subsistence P quota	0.002,0.003	molP $molC^{-1}$
α_i	Chl. sp. slope of P-I curve	9.0,6.0	gC $gChl^{-1}$ / (molE m^{-2})
w'_p	Maximum potential sinking rate	4.0,0.2	m d^{-1}
$\theta_{max,i}$	Max. chl:C ratio	0.10,0.07	m^2 gChl/gC^{-1}
γ_i	Exudation fraction	0.05	-
$m1_i$	Linear mortality rate	0.05	d^{-1}
$m2_i$	Quadratic mortality rate	0.001	d^{-1}/(mmolC m^{-3})
$\delta_{S,i}$	Fraction of dead cells diverted to small det.	0.7,1.0	-

https://doi.org/10.5194/bg-2020-1
Preprint. Discussion started: 31 January 2020

Process formulations for the zooplankton module are provided in Table B4.Following Fasham et al. (1990), prescribed preferences of prey items for each zooplankton (Table B6) are dynamically weighed with their relative abundance to determine the effective preferences (B21,B22). Zooplankton are assumed to excrete into DIM pool (B6,B19).

Table B4. Process equations and functional relationships used in the zooplankton module.

X (=C,N,P) Excretion rate of z_j	$z_j^X\_DIX$	$= z_j^C \cdot e_j \cdot f_{T,zoo-j} \cdot QX_j$	(B19)
X (=C,N,P) Mortality rate of z_j	M_j^X	$= z_j^C \cdot (m1_j + z_j^C \cdot m2_j) \cdot QX_j$	(B20)
Ingestion rate of X from t_k	$I_{j,k}^X$	$= I_{max,j} \cdot f_{T,zoo-j} \cdot \frac{pw_{j,k} \cdot t_k^C}{K_j^C + \sum_k (pw_{j,k} \cdot t_k^C)} \cdot QX_k$	(B21)
Weighed preference of target k by j	$pw_{j,k}$	$= pref_{j,k} \cdot t_k^C / \sum_k (pref_{j,k} \cdot t_k^C)$	(B22)
Assimilated X={C,N,P,Si} ingestion of	$t_k^X\_z_j^X$	$= z_j^C \cdot \epsilon_j^X \cdot I_{j,k}^X$	(B23)
Total unass. X={C,N,P,Si} ing. by z_j	U_j^X	$= z_j^C \cdot \sum_k \cdot (1 - \epsilon_j^X) \cdot I_{j,k}^X$	(B24)

As in Kerimoglu et al. (2017b), assimilated and un-assimilated fractions of the ingested prey by each zooplankton j are determined by the assimilation efficiency ϵ_j^X (B23),B24), which is continuously adjusted (as in Grover, 2002), such that the zooplankton can maintain their homeostatic elemental composition. Here this scheme was extended to multiple nutrients, i.e., N and P, and ϵ^X are calculated iteratively, similar to that in (Kerimoglu et al., 2018). Starting from each ϵ^X set to default values (Table B5), if P to be ingested would be less than the amount required to match the ingested C, ϵ^C is down-regulated, and vice versa:

$$\epsilon^P = \frac{\epsilon_j^C \cdot \sum_k I_{j,k}^C \cdot QP_j}{\sum_k I_{j,k}^P}, \quad \text{if } \epsilon_j^P \cdot \sum_k I_{j,k}^P > \epsilon_j^C \cdot \sum_k I_{j,k}^C \cdot QP_j \tag{B25}$$

$$\epsilon^C = \frac{\epsilon_j^P \cdot \sum_k I_{j,k}^P}{\sum_k I_{j,k}^C \cdot QP_j}, \quad \text{otherwise} \tag{B26}$$

Next, following the same logic, ϵ^N and ϵ^C are regulated to match the C- and N-intake according to the QN_j

$$\epsilon^N = \frac{\epsilon_j^C \cdot \sum_k I_{j,k}^C \cdot QN_j}{\sum_k I_{j,k}^N}, \quad \text{if } \epsilon_j^N \cdot \sum_k I_{j,k}^N > \epsilon_j^C \cdot \sum_k I_{j,k}^C \cdot QN_j \tag{B27}$$

$$\epsilon^C = \frac{\epsilon_j^N \cdot \sum_k I_{j,k}^N}{\sum_k I_{j,k}^C \cdot QN_j}, \quad \text{otherwise} \tag{B28}$$

Finally, ϵ^P is adjusted again, as a potential modification of ϵ^C in (B27) may require an updated P-intake:

$$\epsilon^P = \frac{\epsilon_j^C \cdot \sum_k I_{j,k}^C \cdot QP_j}{\sum_k I_{j,k}^P}, \quad \text{if } \epsilon_j^P \cdot \sum_k I_{j,k}^P > \epsilon_j^C \cdot \sum_k I_{j,k}^C \cdot QP_j \tag{B29}$$

https://doi.org/10.5194/bg-2020-1
Preprint. Discussion started: 31 January 2020

Table B5. Parameters of the zooplankton module. Where necessary, multiple values were provided for micro- and meso-zooplankton.

Symbol	Description	Value$_j$	Unit
$I_{max,j}$	Maximum ingestion rate	1.8,1.5	-
K_j^C	Half saturation constant	15.0,20.0	-
Q_j^N	Constant N:C ratio of z_j	0.15	molN molC^{-1}
Q_j^P	Constant P:C ratio of z_j	0.0094	molP molC^{-1}
ϵ_j^C	C Assimilation efficiency	0.5,0.4	-
$\epsilon_j^{N,P}$	N&P Assimilation efficiency	0.8,0.8	-
e_j	Excretion rate	0.05	d^{-1}
$m1_j$	Linear mortality rate	0.02	d^{-1}
$m2_j$	Quadratic mortality rate	0.01,0.02	d^{-1}/(mmolC m^{-3})
$\delta_{S,j}$	Fraction of mort. & unass. ing. diverted to small det.	0.85,0.7	-
δ_{dom}	Fraction of DOM in unassimilated ingestion	0.8	-

Table B6. Grazing preferences $pref_{j,k}$ of predator j (rows) for target t_k (columns).

	det_S	p_{nf}	p_d	z_{mic}
z$_{mic}$	0.4	0.5	0.1	-
z$_{mes}$	-	0.3	0.1	0.6

B2 Abiotic component

B2.1 Organic material and nutrients

The abiotic components, describe the geochemical transformation between various organic and inorganic pools (DIM, DOM, small and large detritus classes, O2 and the particulate organic matter in the benthos (B-POM), see Fig. 2). Model structure used here is simplified from ECOHAM (Lorkowski et al., 2012), by excluding carbonate and bacterial dynamics. Coupling of the abiotic component with the planktonic components are mediated through the uptake of DIM by phytoplankton (B3,B4), and the recycling of the dead and surplus material. The unassimilated fraction of the ingestions by zooplankton are distributed into the DOM (B35) and the two detritus pools as in Lorkowski et al. (2012). For X=C,N,P, mortality of plankton (B18,B20) are distributed into the small and large detritus classes (B36,B37). For Si, there are no DOM or det$_S^{Si}$ pools (Fig.2), therefore all diatom mortality and Si bound to the ingested diatoms are diverted to the det$_L^{Si}$ (B38).

Conversion of areal units (mmolX/m^2/d) of the surface and bottom flux terms (B52-B56) to volumetric units (mmolX/m^3/d) required for the pelagic variables is handled by the FABM coupler through division by the surface and bottom layer thicknesses ($\Delta z(s)$, $\Delta z(b)$) internally, which are specified here but not in the model codes.

https://doi.org/10.5194/bg-2020-1
Preprint. Discussion started: 31 January 2020

Biogeosciences Discussions Open Access EGU

Table B7. Source-sink terms of the dynamic variables (all in mmol/m^3/d, except for the benthic variables (B39-B40) in mmol/m^2/d) of the abiotic module. Description of processes or functional relationships and parameters are provided in Tables B9 and B8, respectively.

DINO3	$s(DINO3)$	$= DINH4\_DINO3 - \sum_i DINO3\_p_i^N - DINO3\_BPOM/\Delta z(b) - DINO3\_N2$	(B30)
DINH4	$s(DINH4)$	$= BPON\_DINH4/\Delta z(b) + DON\_DINH4 + sum_j z_j^N\_DIN - \sum_i DINH4\_p_i^N - DINH4\_DINO3$	(B31)
DIP	$s(DIP)$	$= BPOP\_DIP/\Delta z(b) + DOP\_DIP + sum_j z_j^P\_DIP - \sum_i DIP\_p_i^P$	(B32)
DISi	$s(DISi)$	$= BPOSi\_DISi/\Delta z(b) + det_L^{Si}\_DISi - \sum_i DISi\_p_i^{Si})$	(B33)
O2	$s(O2)$	$= air\_O2/\Delta z(s) + \sum_i p_i\_O2 - \sum_j O2\_z_j - O2\_DOM - O2\_DINH4 - O2\_BPOM$	(B34)
Diss. org. X={C,N,P}	$s(DOX)$	$= \sum_i p_i^X\_DOX + \sum_j(\delta_{dom} \cdot U_j^X) + \sum_{C=S,L} det_C^X\_DOX - DOX\_DIX$	(B35)
Small det. X={C,N,P}	$s(det_S^X)$	$= \sum_i(\delta_{S,i} \cdot M_i^X) + \sum_j(\delta_{S,j} \cdot ((1-\delta_{dom}) \cdot U_j^X + M_j^X) - det_S^X\_DOX - det_S^X\_BPOX/\Delta z(b)$	(B36)
Large det. X={C,N,P}	$s(det_L^X)$	$= \sum_i((1-\delta_{S,i}) \cdot M_i^X) + \sum_j((1-\delta_{S,j}) \cdot ((1-\delta_{dom}) \cdot U_j^X + M_j^X) - det_L^X\_DOX - det_L^X\_BPOX/\Delta z(b)$	(B37)
Large det. Si	$s(det_L^{Si})$	$= \sum_i(M_i^{Si}) + \sum_j U_j^{Si} - det_L^{Si}\_DISi - det_L^{Si}\_BPOSi/\Delta z(b)$	(B38)
Benthic-POX={C,P,Si}	$s(BPOX)$	$= \sum_{c=S,L} det_c^X\_BPOX - BPOX\_DIX$	(B39)
Benthic-PON	$s(BPON)$	$= \sum_{c=S,L} det_c^N\_BPON - BPON\_DINH4 - BPON\_N2$	(B40)

Table B8. Parameters of the abiotic module.

Symbol	Description	Value(C,N,P,Si)	Unit
λ^X	Rem. rate of DOM	0.05	d^{-1}
$r_S^{N,P}$	Decay rate of N&P in small det.	0.12	d^{-1}
r_S^C	Decay rate of C in small det.	$r_S^{N,P} \cdot 0.85$	d^{-1}
$r_L^{N,P}$	Decay rate of N&P in large det.	0.1	d^{-1}
r_L^C	Decay rate of C in large det.	$r_S^{N,P} \cdot 0.85$	d^{-1}
r_L^Si	Decay rate of Si in large det.	$r_S^{N,P} \cdot 0.085$	d^{-1}
r_{nit}	Nitrification rate	0.05	d^{-1}
QN_b	Bacterial N:C ratio	0.2	molN/molC
w_{detS}	Sinking rate of small det.	2.0	m d^{-1}
w_{detL}	Sinking rate of large det.	10.0	m d^{-1}
br^C	Benthic rem. rate of C	0.028	d^{-1}
$br^{N,P}$	Benthic rem. rate N&P	0.0333	d^{-1}
br^Si	Benthic rem. rate of Si	0.0130	d^{-1}
ρ_{Seitz}	Denit./O2 cons. prop. constant	0.116	molN/molO2
ω_{detS}	Sed. rate of small det.	0.5	m d^{-1}
ω_{detL}	Sed. rate of large det.	5.0	m d^{-1}

https://doi.org/10.5194/bg-2020-1
Preprint. Discussion started: 31 January 2020

Biogeosciences Discussions Open Access EGU

Table B9. Process equations and functional relationships used in the abiotic module.

O2 switch	SW_{O2}	if $O2 > 0.0$ $= 1.0$, else $= 0.0$	(B41)
NO3 switch	SW_{NO3}	if $DINO3 > 0.0$ $= 1.0$, else $= 0.0$	(B42)
Remineralization of DOX	DOX_DIX	$= f_{T,abio} \cdot \lambda^X \cdot DOX$	(B43)
Decay of X={C,N,P} in det_S	$det_S^X\_DOX$	$= f_{T,abio} \cdot r_S^X \cdot\ det_S^X$	(B44)
Decay of of X={C,N,P,Si} in det_L	$det_L^X\_DOX$	$= f_{T,abio} \cdot r_L^X \cdot\ det_L^X$	(B45)
Nitrification of pelagic NH4	$DINH4\_DINO3$	$= SW_{O2} \cdot f_{T,abio} \cdot DINH4 \cdot r_{nit}$	(B46)
Denitrification in water	$DINO3\_N2$	$= 0.5 \cdot (1 - SW_{O2}) \cdot SW_{NO3} \cdot DOC\_DIC \cdot QN_b$	(B47)
O2 production by p_i	p_i_O2	$= DIC\_p_i^C \cdot 1.0$[molO2/molC]	(B48)
O2 consumption by z_j	$O2\_z_j$	$= z_j^C\_DIC \cdot 1.0$[molO2/molC]	(B49)
O2 consumption by remin.	$O2\_DOM$	$= SW_{O2} \cdot DOC\_DIC + (1 - SW_{O2}) \cdot (1 - SW_{NO3}) \cdot DOC\_DIC$	(B50)
O2 consumption by nitrif.	$O2\_DINH4$	$= DINH4\_DINO3 \cdot 2.0[molO2/molN]$	(B51)
O2 flux from air	air_O2	$= k(O2_0 - O2)$, k from Wanninkhof (1992), $O2_0$ from UNESCO (1986)	(B52)
Sedimentation of det_S^X	$det_S^X\_BPOX$	$= \omega_{detL} \cdot det_S^X$	(B53)
Sedimentation of det_L^X	$det_L^X\_BPOX$	$= \omega_{detS} \cdot det_L^X$	(B54)
Benthic X={C,P,Si} remin.	$BPOX\_DIX$	$= br^X \cdot BPOX$	(B55)
Benthic O2 consumption	$O2\_BPOM$	$= SW_{O2(b)} \cdot BPOC\_DIC + (1 - SW_{O2(b)}) \cdot (1 - SW_{NO3(b)}) \cdot BPOC\_DIC$	(B56)
Potential benthic denit.	$BPON\_N2'$	$= \rho_{Seitz} \cdot O2\_BPOM$	(B57)
Benthic denitrification	$BPON\_N2$	$= BPON\_N2' - \max(0.0, BPON\_N2' - BPON\_DINH4')$	(B58)
Potential benthic N remin.	$BPON\_DINH4'$	$= br^N \cdot BPON$	(B59)
Benthic N remineralization	$BPON\_DINH4$	$= \max(0.0, BPON\_DINH4' - BPON\_N2')$	(B60)
Benthic NO3 reduction	$DINO3\_BPOM$	$= 0.5 \cdot SW_{O2} \cdot SW_{NO3} \cdot BPON\_DINH4$	(B61)

B2.2 Light

In GETM, light intensity at a given depth, $I(z)$, is described by:

$$I(z) = I_0 \cdot a \cdot \exp(-\frac{z}{\eta_1}) + I_0 \cdot (1-a) \cdot \exp(-\frac{z}{\eta_2} - \int_z^0 \sum_n K_n(z')dz') \quad \text{(B62)}$$

where, I_0 is the light at the water surface, a, η_1 and $\eta 2$ describe the attenuation of the red and blue-green spectra, and K_n describe various constituents in the water, i.e., phytoplankton, detritus, DOC and SPM. For the former three, concentrations of which are explicitly modelled, $K_n = k_n \cdot C_n$, where C_n is the concentration of constituent n, and k_n is the specific attenuation coefficients, which are set to $k_{p_i^C}$ =0.015, k_{det^C} =0.01 and k_{DOC} =0.002 m^2 mmolC^1 (Oubelkheir et al., 2005; Stedmon et al.,

https://doi.org/10.5194/bg-2020-1
Preprint. Discussion started: 31 January 2020

2001). For describing the contribution of SPM, K_{SPM}, which is not explicitly modeled here, we use an analytical function of the form:

$$K_{SPM} = K'_{SPM} \cdot f_{SPM}(z) \cdot f_{SPM}(t) \tag{B63}$$

where, the K'_{SPM} is the maximum potential attenuation, $f_{SPM}(z_{max})$ (z_{max}: bottom depth) is a sigmoidal function of depth to account for the cross-shore variations and $f_{SPM}(t)$ (t: day of year) is a sinusoidal function to account for the cyclic seasonal variations driven by the riverine discharges at the coastal region and thermal stratification offshore:

$$f_{SPM}(z_{max}) = fz_{minfr} + (1.0 - fz_{minfr}) * (1.0 - 1.0/(1.0 + \exp(z *_{max} - z_{max} * 0.5))) \tag{B64}$$

$$f_{SPM}(t) = F * (A * sin(2.0 \cdot t \cdot \pi/365.0 + 2.0 \cdot L \cdot \pi/365.0) + B) \tag{B65}$$

Based on an analysis (see Kerimoglu, 2014) of the temporally and spatially variable SPM data collected by a Scanfish device (see Maerz et al. (2016) for a description of the data set), and the model performance, we fitted $K'_{SPM} = 1.5$, $fz_{minfr} = 0.3$, $z*_{max} = 7.5$ and $F = 0.05$, $A = 6.0$, $B = 12.0$, $L = 85.0$ for $f_{SPM}(t)$. Finally, for the parameterization of a, η_1 and $\eta 2$, we specify the Jerlov Type-1 option in GETM , which corresponds to clear ocean waters (Paulson and Simpson, 1977), given that we explicitly take the attenuation by organic and SPM constituents into account.

Author contributions. OK designed the study with contributions from YV, developed the biogeochemical model, performed the model skill assessment and conducted the model-based analyses with contributions by FC and prepared the first draft of the manuscript. JvB provided the monthly average nutrient concentrations, and YV assisted the compilation of the monitoring data. RH and KK assisted the improvement of the hydrodynamical model with horizontal diffusion. All co-authors contributed to the discussion of the results and revisions of the manuscript.

Competing interests. The authors declare that no competing interests are present.

Acknowledgements. OK was supported by the German Environment Agency, UBA [3718252110] and German Science Foundation, DFG [KE 1970/1-1 and KE 1970/2-1]. OK and FC was supported by the German Federal Ministry of Research and Education, BMBF [03F0740B]. KK was financed by the Collaborative Research Centre of the DFG, TRR 181 [274762653]. Data at Helgoland were provided by Alfred Wegener Institute (AWI), and at Norderelbe, Suederpiep and Westerhever were provided by the Landesamt für Landwirtschaft, Umwelt und ländliche Räume des Landes Schleswig Holstein. Noordwijk and Terschelling data were provided by the Rijkswaterstaat. Simulations were performed on the 'Mistral' supercomputer of the German Climate Computing Center (DKRZ). We thank Johannes Pätsch (Uni. Hamburg) for providing the boundary conditions and ECOHAM code that helped developing the abiotic component of the model, Sonja van Leeuwen (NIOZ) for providing the riverine data, Wilhelm Petersen, Gisbert Breitbach and KOI group of the HZG for the acquisition and maintenance of the FerryBox and COSYNA data and Ivan Kuznetsov (then at HZG) for the cooperation on model validation. OK is grateful to the developers of the open source platforms and free software that made this work possible, foremost, GETM, GOTM, FABM, NetCDF, NCO, Python, Kubuntu OS and UNIX tools.

https://doi.org/10.5194/bg-2020-1
Preprint. Discussion started: 31 January 2020

Appendix: References

Androsov, A., Fofonova, V., Kuznetsov, I., Danilov, S., Rakowsky, N., Harig, S., Brix, H., and Wiltshire, K. H.: FESOM-C : coastal dynamics on hybrid unstructured meshes, Geoscientific Model Development, 12, 1009–1028, https://doi.org/10.5194/gmd-2018-112, 2019.

Backhaus, J. O.: A three-dimensional model for the simulation of shelf sea dynamics, Deutsche Hydrographische Zeitschrift, 38, 165–187, https://doi.org/10.1007/BF02328975, 1985.

Barthel, K., Daewel, U., Pushpadas, D., Schrum, C., Årthun, M., and Wehde, H.: Resolving frontal structures: on the payoff using a less diffusive but computationally more expensive advection scheme, Ocean Dynamics, 62, 1457–1470, https://doi.org/10.1007/s10236-012-0578-9, 2012.

Becker, E. and Burkhardt, U.: Nonlinear Horizontal Diffusion for GCMs, Monthly Weather Review, 135, 1439–1454, https://doi.org/10.1175/MWR3348.1, 2007.

Becker, G., Dick, S., and Dippner, J.: Hydrography of the German Bight, Marine Ecology Progress Series, 91, 9–18, 1992.

Beckers, J.-M., Burchard, H., Deleersnijder, E., and Mathieu, P.: Numerical Discretization of Rotated Diffusion Operators in Ocean Models, Monthly Weather Review, 128, 2711–2733, 2000.

Beddig, S., Brockmann, U., Dannecker, W., Körner, D., Pohlmann, T., Puls, W., Radach, G., Rebers, A., H-J., R., Schatzmann, M., Schlünzen, H., and Schulz, M.: Nitrogen Fluxes in the German Bight, Marine Pollution Bulletin, 34, 382–394, 1997.

Beniston, M., Stephenson, D. B., Christensen, O. B., Ferro, C. a. T., Frei, C., Goyette, S., Halsnaes, K., Holt, T., Jylhä, K., Koffi, B., Palutikof, J., Schöll, R., Semmler, T., and Woth, K.: Future extreme events in European climate: an exploration of regional climate model projections, Climatic Change, 81, 71–95, https://doi.org/10.1007/s10584-006-9226-z, 2007.

Breitbach, G., Krasemann, H., Behr, D., Beringer, S., Lange, U., and Vo, N.: Accessing diverse data comprehensively – CODM , the COSYNA data portal, Ocean Science, 12, 909–923, https://doi.org/10.17616/R3K02T, 2016.

Bruggeman, J. and Bolding, K.: A general framework for aquatic biogeochemical models, Environmental Modelling & Software, 61, 249–265, https://doi.org/10.1016/j.envsoft.2014.04.002, 2014.

Burchard, H. and Badewien, T. H.: Thermohaline residual circulation of the Wadden Sea, Ocean Dynamics, 65, 1717–1730, https://doi.org/10.1007/s10236-015-0895-x, 2015.

Burchard, H. and Bolding, K.: GETM: A general estuarine transport model, Tech. rep., Joint Research Centre, Ispra, Italy, 2002.

Burchard, H. and Hetland, R. D.: Quantifying the Contributions of Tidal Straining and Gravitational Circulation to Residual Circulation in Periodically Stratified Tidal Estuaries, Journal of Physical Oceanography, 40, 1243–1262, https://doi.org/10.1175/2010JPO4270.1, 2010.

Burchard, H. and Rennau, H.: Comparative quantification of physically and numerically induced mixing in ocean models, Ocean Modelling, 20, 293–311, https://doi.org/10.1016/j.ocemod.2007.10.003, 2008.

Burchard, H., Flöser, G., Staneva, J. V., Badewien, T. H., and Riethmüller, R.: Impact of Density Gradients on Net Sediment Transport into the Wadden Sea, Journal of Physical Oceanography, 38, 566–587, https://doi.org/10.1175/2007JPO3796.1, 2008.

Burchard, H., Schuttelaars, H. M., and Ralston, D. K.: Sediment Trapping in Estuaries, Annual Review of Marine Science, 10, 371–395, https://doi.org/10.1146/annurev-marine-010816-060535, 2018.

Callies, U. and Scharfe, M.: Mean spring conditions at Helgoland Roads, North Sea: Graphical modeling of the influence of hydro-climatic forcing and Elbe River discharge, Journal of Sea Research, 101, 1–11, https://doi.org/10.1016/j.seares.2014.06.008, 2015.

Callies, U., Gaslikova, L., Kapitza, H., and Scharfe, M.: German Bight residual current variability on a daily basis: principal components of multi-decadal barotropic simulations, Tech. rep., https://doi.org/10.1007/s00367-016-0466-2, 2016.

https://doi.org/10.5194/bg-2020-1
Preprint. Discussion started: 31 January 2020

Callies, U., Gaslikova, L., Kapitza, H., and Scharfe, M.: German Bight residual current variability on a daily basis: principal components of multi-decadal barotropic simulations, Geo-Marine Letters, 37, 151–162, https://doi.org/10.1007/s00367-016-0466-2, 2017.

Carpenter, J. R., Merckelbach, L., Callies, U., Clark, S., Gaslikova, L., and Baschek, B.: Potential Impacts of Offshore Wind Farms on North Sea Stratification, PloS one, 11, e0160 830, https://doi.org/10.1594/WDCC/coastDat-2, 2016.

Chegini, F., Holtermann, P., Kerimoglu, O., Becker, M., Kreus, M., Klingbeil, K., Gräwe, U., Winter, C., and Burchard, H.: Processes of stratification and de-stratification during an extreme river discharge event in the German Bight in a model study, Journal of Geophysical Research : Oceans, submitted.

Cloern, J. E., Foster, S. Q., and Kleckner, A. E.: Phytoplankton primary production in the world's estuarine-coastal ecosystems, Biogeosciences, 11, 2477–2501, https://doi.org/10.5194/bg-11-2477-2014, 2014.

Daewel, U., Schrum, C., and Macdonald, J. I.: Towards end-to-end (E2E) modelling in a consistent NPZD-F modelling framework (ECOSMO E2E_v1.0): application to the North Sea and Baltic Sea, Geoscientific Model Development, 12, 1765–1789, 2019.

Dippner, J. W.: A frontal-resolving model for the German Bight, Continental Shelf Research, 13, 49–66, 1993.

Dolch, T., Buschbaum, C., and Reise, K.: Persisting intertidal seagrass beds in the northern Wadden Sea since the 1930s, Journal of Sea Research, 82, 134–141, https://doi.org/10.1016/j.seares.2012.04.007, http://dx.doi.org/10.1016/j.seares.2012.04.007, 2013.

Emeis, K. C., van Beusekom, J., Callies, U., Ebinghaus, R., Kannen, A., Kraus, G., Kröncke, I., Lenhart, H., Lorkowski, I., Matthias, V., Möllmann, C., Pätsch, J., Scharfe, M., Thomas, H., Weisse, R., and Zorita, E.: The North Sea - A shelf sea in the Anthropocene, Journal of Marine Systems, 141, 18–33, https://doi.org/10.1016/j.jmarsys.2014.03.012, 2015.

Fasham, M., Ducklow, H., and Mckelvie, S.: A nitrogen-based model of plankton dynamics in the oceanic mixed layer, Journal of Marine Research', 48, 591–639, 1990.

Fennel, K. and Testa, J. M.: Biogeochemical Controls on Coastal Hypoxia, Annual Review of Marine Science, 11, 4.1–4.26, https://doi.org/10.1146/annurev-marine-010318-095138, 2019.

Flöser, G., Burchard, H., and Riethmüller, R.: Observational evidence for estuarine circulation in the German Wadden Sea, Continental Shelf Research, 31, 1633–1639, https://doi.org/http://dx.doi.org/10.1016/j.csr.2011.03.014, 2011.

Flynn, K. J.: Modelling multi-nutrient interactions in phytoplankton; balancing simplicity and realism, Progress in Oceanography, 56, 249–279, https://doi.org/10.1016/S0079-6611(03)00006-5, 2003.

Ford, D. A., van der Molen, J., Hyder, K., Bacon, J., Barciela, R., Creach, V., McEwan, R., Ruardij, P., and Forster, R.: Observing and modelling phytoplankton community structure in the North Sea: can ERSEM-type models simulate biodiversity?, Biogeosciences, 14, 1419–1444, https://doi.org/10.5194/bg-2016-304, http://www.biogeosciences-discuss.net/bg-2016-304/, 2017.

Frey, H.: Stratification during periods of oxygen deficiency in the German Bight during the summers from 1981 to 1983: a comparison with the long-term variation in stratification., Meeresforschung, 32, 306–328, 1990.

Garnier, J., Riou, P., Gendre, R. L., Ramarson, A., Billen, G., Cugier, P., Shapira, M., Théry, S., Thieu, V., and Alain, M.: Managing the Agri-Food System of Watersheds to Combat Coastal Eutrophication: A Land-to-Sea Modelling Approach to the French Coastal English Channel, Geosciences, 9, https://doi.org/10.3390/geosciences9100441, 2019.

Gaslikova, L. and Weisse, R.: coastDat-2 TRIM-NP-2d Tide-Surge North Sea, Tech. rep., WDCC at DKRZ, https://doi.org/10.1594/WDCC/coastDat-2_TRIM-NP-2d, 2013.

Gayer, G., Dick, S., Pleskachevsky, A., and Rosenthal, W.: Numerical modeling of suspended matter transport in the North Sea, Ocean Dynamics, 56, 62–77, https://doi.org/10.1007/s10236-006-0070-5, 2006.

https://doi.org/10.5194/bg-2020-1
Preprint. Discussion started: 31 January 2020

Geider, R., MacIntyre, H., and Kana, T.: Dynamic model of phytoplankton growth and acclimation: responses of the balanced growth rate and the chlorophyll a:carbon ratio to light, nutrient-limitation and temperature, Marine Ecology Progress Series, 148, 187–200, 1997.

Gent, P. R. and McWilliams, J. C.: Isopycnal mixing in ocean circulation models, Journal of Physical Oceanography, 20, 150–155, 1990.

Geyer, B.: High-resolution atmospheric reconstruction for Europe 1948–2012: coastDat2, Earth System Science Data, 6, 147–164, https://doi.org/doi:10.5194/essd-6-147-2014, 2014.

Geyer, W. R. and Maccready, P.: The Estuarine Circulation, Annual Review of Fluid Mechanics, 46, 175–197, https://doi.org/10.1146/annurev-fluid-010313-141302, 2014.

Gräwe, U., Flöser, G., Gerkema, T., Duran-Matute, M., Badewien, T., Schulz, E., and Burchard, H.: A numerical model for the entire Wadden Sea: skill assessment and analysis of hydrodynamics, Journal of Geophysical Research: Oceans, 121, 5231–2551, https://doi.org/10.1002/2016JC011655, 2016.

Griffies, S. M. and Hallberg, R. W.: Biharmonic Friction with a Smagorinsky-Like Viscosity for Use in Large-Scale Eddy-Permitting Ocean Models, Monthly Weather Review, 128, 2935–2946, 2000.

Große, F., Greenwood, N., Kreus, M., Lenhart, H. J., Machoczek, D., Pätsch, J., Salt, L. A., and Thomas, H.: Looking beyond stratification: a model-based analysis of the biological drivers of oxygen deficiency in the North Sea, Biogeosciences, 13, 2511–2535, https://doi.org/10.5194/bgd-12-12543-2015, 2016.

Große, F., Kreus, M., Lenhart, H.-J., Pätsch, J., and Pohlmann, T.: A Novel Modeling Approach to Quantify the Influence of Nitrogen Inputs on the Oxygen Dynamics of the North Sea, Frontiers in Marine Science, 4, 1–21, https://doi.org/10.3389/fmars.2017.00383, 2017.

Grover, J.: Stoichiometry, Herbivory and Competition for Nutrients: Simple Models based on Planktonic Ecosystems, J. Theoret. Biol., 214, 599–618, https://doi.org/10.1006/jtbi.2001.2488, 2002.

Hickel, W., Mangelsdorf, P., and Berg, J.: The human impact in the German Bight: Eutrophication during three decades (1962-1991), Helgoländer Meeresuntersuchungen, 47, 243–263, https://doi.org/10.1007/BF02367167, 1993.

Hickey, B. M., Kudela, R. M., Nash, J. D., Bruland, K. W., Peterson, W. T., MacCready, P., Lessard, E. J., Jay, D. a., Banas, N. S., Baptista, a. M., Dever, E. P., Kosro, P. M., Kilcher, L. K., Horner-Devine, a. R., Zaron, E. D., McCabe, R. M., Peterson, J. O., Orton, P. M., Pan, J., and Lohan, M. C.: River Influences on Shelf Ecosystems: Introduction and synthesis, Journal of Geophysical Research, 115, C00B17, https://doi.org/10.1029/2009JC005452, 2010.

Hofmeister, R., Beckers, J.-M., and Burchard, H.: Realistic modelling of the exceptional inflows into the central Baltic Sea in 2003 using terrain-following coordinates, Ocean Modelling, 39, 233–247, https://doi.org/10.1016/j.ocemod.2011.04.007, 2011.

Hofmeister, R., Flöser, G., and Schartau, M.: Estuary-type circulation as a factor sustaining horizontal nutrient gradients in freshwater-influenced coastal systems, Geo-Marine Letters, 37, 179–192, https://doi.org/10.1007/s00367-016-0469-z, 2017.

Holt, J. T. and James, I. D.: An assessment of the fine-scale eddies in a high-resolution model of the shelf seas west of Great Britain, Ocean Modelling, 13, 271–291, https://doi.org/10.1016/j.ocemod.2006.02.005, 2006.

Izett, J. G. and Fennel, K.: Estimating the Cross-Shelf Export of Riverine Materials: Part 2. Estimates of Global Freshwater and Nutrient Export, Global Biogeochemical Cycles, 32, 176–186, https://doi.org/10.1002/2017GB005668, 2018.

Kantha, L. H. and Clayson, C. A.: Numerical models of oceans and oceanic processes, Academic Press, 2000.

Kerimoglu, O.: Parameterization of turbidity in the German Bight, Tech. rep., Helmholtz-Zentrum Geesthacht, Geesthacht, 2014.

Kerimoglu, O., Hofmeister, R., Maerz, J., Riethmüller, R., and Wirtz, K. W.: The acclimative biogeochemical model of the southern North Sea, Biogeosciences, 14, 4499–4531, https://doi.org/10.5194/bg-14-4499-2017, 2017a.

https://doi.org/10.5194/bg-2020-1
Preprint. Discussion started: 31 January 2020

Kerimoglu, O., Jacquet, S., Vinçon-Leite, B., Lemaire, B. J., Rimet, F., Soulignac, F., Trévisan, D., and Anneville, O.: Modelling the plankton groups of the deep, peri-alpine Lake Bourget, Ecological Modelling, 359, 415–433, https://doi.org/10.1016/j.ecolmodel.2017.06.005, 2017b.

Kerimoglu, O., Große, F., Kreus, M., Lenhart, H.-J., and van Beusekom, J. E.: A model-based projection of historical state of a coastal ecosystem: relevance of phytoplankton stoichiometry, Science of the Total Environment, 639, 1311–1323, https://doi.org/10.1016/j.scitotenv.2018.05.215, 2018.

Klingbeil, K., Mohammadi-Aragh, M., Gräwe, U., and Burchard, H.: Quantification of spurious dissipation and mixing – Discrete variance decay in a Finite-Volume framework, Ocean Modelling, 81, 49–64, https://doi.org/10.1016/j.ocemod.2014.06.001, 2014.

Lenhart, H., Radach, G., and Ruardij, P.: The effects of river input on the ecosystem dynamics in the continental coastal zone of the North Sea using ERSEM, Journal of Sea Research, 38, 249–274, 1997.

Loebl, M., Colijn, F., van Beusekom, J., Baretta-Bekker, J., Lancelot, C., Philippart, C., Rousseau, V., and Wiltshire, K.: Recent patterns in potential phytoplankton limitation along the Northwest European continental coast, Journal of Sea Research, 61, 34–43, https://doi.org/10.1016/j.seares.2008.10.002, 2009.

Lorkowski, I., Pätsch, J., Moll, A., and Kühn, W.: Interannual variability of carbon fluxes in the North Sea from 1970 to 2006 - Competing effects of abiotic and biotic drivers on the gas-exchange of CO 2, Estuarine, Coastal and Shelf Science, 100, 38–57, https://doi.org/10.1016/j.ecss.2011.11.037, 2012.

Los, F., Villars, M., and Van der Tol, M.: A 3-dimensional primary production model (BLOOM/GEM) and its applications to the (southern) North Sea (coupled physical–chemical–ecological model), Journal of Marine Systems, 74, 259–294, https://doi.org/10.1016/j.jmarsys.2008.01.002, 2008.

Maerz, J., Hofmeister, R., van der Lee, E. M., Gräwe, U., Riethmüller, R., and Wirtz, K. W.: Maximum sinking velocities of suspended particulate matter in a coastal transition zone, Biogeosciences, 13, 4863–4876, https://doi.org/10.5194/bg-13-4863-2016, 2016.

Merz, B., Elmer, F., Kunz, M., Mühr, B., Schröter, K., and Uhlemann-Elmer, S.: The extreme flood in June 2013 in Germany, La Houille Blanche, 1, 5–10, https://doi.org/10.1051/lhb/2014001, http://www.shf-lhb.org/10.1051/lhb/2014001, 2014.

Morel, F.: Kinetics of nutrient uptake and growth in phytoplankton, Journal of Phycology, 23, 137–150, 1987.

Nasermoaddeli, M. H., Lemmen, C., Stigge, G., Kerimoglu, O., Burchard, H., Klingbeil, K., Hofmeister, R., Kreus, M., Wirtz, K. W., and F, K.: A model study on the large-scale effect of macrofauna on the suspended sediment concentration in a shallow shelf sea, Estuarine, Coastal and Shelf Science, pp. 1–15, https://doi.org/10.1016/j.ecss.2017.11.002, 2017.

OSPAR: Eutrophication Status of the OSPAR Maritime Area. Third Integrated Report on the Eutrophication Status of the OSPAR Maritime Area Submitted by ICG-EMO, Tech. rep., 2017.

Oubelkheir, K., Sciandra, A., and Babin, M.: Bio-optical and biogeochemical properties of different trophic regimes in oceanic waters, Limnology and Oceanography, 50, 1795–1809, https://doi.org/10.4319/lo.2005.50.6.1795, 2005.

Pätsch, J. and Kühn, W.: Nitrogen and carbon cycling in the North Sea and exchange with the North Atlantic—A model study. Part I. Nitrogen budget and fluxes, Continental Shelf Research, 28, 767–787, https://doi.org/10.1016/j.csr.2007.12.013, 2008.

Pätsch, J., Burchard, H., Dieterich, C., Gräwe, U., Gröger, M., Mathis, M., Kapitza, H., Bersch, M., Moll, A., Pohlmann, T., Su, J., Ho-Hagemann, H. T., Schulz, A., Elizalde, A., and Eden, C.: An evaluation of the North Sea circulation in global and regional models relevant for ecosystem simulations, Ocean Modelling, 116, 70–95, https://doi.org/10.1016/j.ocemod.2017.06.005, 2017.

Paulson, C. and Simpson, J.: Irradience measurements in the upper ocean, Journal of Physical Oceanography, 7, 952–956, 1977.

https://doi.org/10.5194/bg-2020-1
Preprint. Discussion started: 31 January 2020

Pein, J., Eisele, A., Hofmeister, R., Sanders, T., Daewel, U., Stanev, E. V., Beusekom, J. V., Staneva, J., and Schrum, C.: Nitrogen cycling in the Elbe estuary from a joint 3D-modelling and observational perspective, Biogeosciences Discussions, pp. 1–34, 2019.

Petersen, W., Schroeder, F., and Bockelmann, F.-D.: FerryBox - Application of continuous water quality observations along transects in the North Sea, Ocean Dynamics, 61, 1541–1554, https://doi.org/10.1007/s10236-011-0445-0, http://link.springer.com/10.1007/s10236-011-0445-0, 2011.

Pietrzak, J.: The Use of TVD Limiters for Forward-in-Time Upstream-Biased Advection Schemes in Ocean Modeling, Monthly Weather Review, 126, 812–830, 1998.

Platis, A., Siedersleben, S. K., Bange, J., Lampert, A., Bärfuss, K., Hankers, R., Cañadillas, B., Foreman, R., Schulz-stellenfleth, J., Djath, B., Neumann, T., and Emeis, S.: First in situ evidence of wakes in the far field behind offshore wind farms, Scientific Reports, 8, 2163, https://doi.org/10.1038/s41598-018-20389-y, 2018.

Pohlmann, T.: A meso-scale model of the central and southern North Sea: Consequences of an improved resolution, Continental Shelf Research, 26, 2367–2385, https://doi.org/10.1016/j.csr.2006.06.011, 2006.

Radach, G.: Ecosystem Functioning in the German Bight Under Continental Nutrient Inputs by Rivers, Estuaries, 15, 477–496, https://doi.org/10.2307/1352392, 1992.

Radach, G. and Pätsch, J.: Variability of Continental Riverine Freshwater and Nutrient Inputs into the North Sea for the Years 1977 – 2000 and Its Consequences for the Assessment of Eutrophication, Estuaries and Coasts, 30, 66–81, https://doi.org/10.1007/BF02782968, 2007.

Roberts, M. and Marshall, D.: Do We Require Adiabatic Dissipation Schemes in Eddy-Resolving Ocean Models?, Journal of Physical Oceanography, 28, 2050–2063, 1998.

Schrum, C.: Thermohaline stratification and instabilities at tidal mixing fronts: Results of an eddy resolving model for the German Bight, Continental Shelf Research, 17, 689–716, https://doi.org/10.1016/S0278-4343(96)00051-9, 1997.

Sharples, J., Middelburg, J., Fennel, K., and Jickells, T.: What proportion of riverine nutrients reaches the open ocean?, Global Biogeochemical Cycles, 31, 39–58, https://doi.org/10.1002/2016GB005483, 2017.

Siegismund, F. and Schrum, C.: Decadal changes in the wind forcing over the North Sea, Climate Research, 18, 39–45, 2001.

Simpson, J., Bos, W., Schirmer, F., Souza, A., Rippeth, T., Jones, S., and Hydes, D.: Periodic stratification in the Rhine ROFI in the North Sea, Oceanologica Acta, 16, 23–32, 1993.

Smagorinsky, J.: General circulation experiments with the primitive equations. Part I: The basic experiment, Monthly Weather Review, 91, 99–164, https://doi.org/10.1126/science.27.693.594, 1963.

Smith, V. H. and Schindler, D. W.: Eutrophication science: where do we go from here?, Trends in Ecology & Evolution, 24, 201–207, https://doi.org/10.1016/j.tree.2008.11.009, 2009.

Stanev, E. V., Jacob, B., and Pein, J.: German Bight estuaries : An inter-comparison on the basis of numerical modeling, Continental Shelf Research, 174, 48–65, https://doi.org/10.1016/j.csr.2019.01.001, https://doi.org/10.1016/j.csr.2019.01.001, 2019.

Staneva, J., Stanev, E., Wolff, J.-O., Badewien, T., Reuter, R., Flemming, B., Bartholomä, A., and Bolding, K.: Hydrodynamics and sediment dynamics in the German Bight. A focus on observations and numerical modelling in the East Frisian Wadden Sea, Continental Shelf Research, 29, 302–319, https://doi.org/10.1016/j.csr.2008.01.006, 2009.

Stedmon, C., Markager, S., and Kaas, H.: The optics of chromophoric dissolved organic matter (CDOM) in the Greenland Sea: An algorithm for differentiation between marine and terrestrially derived organic matter, Limnology and Oceanography, 46, 2087–2093, https://doi.org/10.4319/lo.2001.46.8.2087, 2001.

https://doi.org/10.5194/bg-2020-1
Preprint. Discussion started: 31 January 2020

Stips, A., Bolding, K., Pohlmann, T., and Burchard, H.: Simulating the temporal and spatial dynamics of the North Sea using the new model GETM (general estuarine transport model), Ocean Dynamics, 54, 266–283, https://doi.org/10.1007/s10236-003-0077-0, http://dx.doi.org/10.1007/s10236-003-0077-0, 2004.

Sündermann, J. and Pohlmann, T.: A brief analysis of North Sea physics, Oceanologia, 53, 663–689, https://doi.org/10.5697/oc.53-3.663, http://linkinghub.elsevier.com/retrieve/pii/S0078323411500193, 2011.

UNESCO: Progress on oceanographic tables and standards 1983–1986: work and recommendations of the UNESCO/SCOR/ICES/IAPSO Joint Panel. Technical Papers in Marine Science, 50., Tech. rep., 1986.

van Aken, H. M.: The onset of seasonal stratification in shelf seas due to differential advection in the presence of a salinity gradient, Continental Shelf Research, 5, 475–485, https://doi.org/10.1016/0278-4343(86)90071-3, 1986.

van Beusekom, J. and Brockmann, U.: Transformation of Phosphorus in the Elbe Estuary, Estuaries, 21, 518–526, 1998.

van Beusekom, J. E., Carstensen, J., Dolch, T., Grage, A., Hofmeister, R., Lenhart, H., Kerimoglu, O., Kolbe, K., Pätsch, J., Rick, J., Rönn, L., and Ruiter, H.: Wadden Sea Eutrophication: Long-Term Trends and Regional Differences, Frontiers in Marine Science, 6, 370, https://doi.org/10.3389/fmars.2019.00370, 2019.

van Leeuwen, S., Tett, P., Mills, D., and Van Der Molen, J.: Stratified and nonstratified areas in the North Sea: Long-term variability and biological and policy implications, Journal of Geophysical Research: Oceans, 120, 4670–4686, https://doi.org/10.1002/2014JC010485, 2015.

Voynova, Y. G., Brix, H., Petersen, W., Weigelt-Krenz, S., and Scharfe, M.: Extreme Flood Impact on Estuarine and Coastal Biogeochemistry: the 2013 Elbe Flood, Biogeosciences, 14, 541–557, https://doi.org/10.5194/bg-2016-218, 2017.

Wang, Y.: Importance of subgrid-scale parameterization in numerical simulations of lake circulation, Advances in Water Resources, 26, 277–294, 2003.

Wanninkhof, R.: Relationship between wind speed and gas exchange over the ocean, Journal of Geophysical Research, 97, 7373–7382, https://doi.org/10.1029/92JC00188, 1992.

Wetz, M. S. and Yoskowitz, D. W.: An 'extreme' future for estuaries ? Effects of extreme climatic events on estuarine water quality and ecology, Marine Pollution Bulletin, 69, 7–18, https://doi.org/10.1016/j.marpolbul.2013.01.020, http://dx.doi.org/10.1016/j.marpolbul.2013.01.020, 2013.

Wiltshire, K. H., Malzahn, A. M., Wirtz, K., Greve, W., Janisch, S., Mangelsdorf, P., Manly, B. F. J., and Boersma, M.: Resilience of North Sea phytoplankton spring bloom dynamics: An analysis of long-term data at Helgoland Roads, Limnology and Oceanography, 53, 1294–1302, https://doi.org/10.4319/lo.2008.53.4.1294, 2008.

Zhang, Y. J., Ye, F., Stanev, E. V., and Grashorn, S.: Seamless cross-scale modeling with SCHISM, Ocean Modelling, 102, 64–81, https://doi.org/10.1016/j.ocemod.2016.05.002, 2016.